energies

MDPI

Article

Integrated Biogas–Hydrogen–PV–Energy Storage–Gas Turbine System: A Pathway to Sustainable and Efficient Power Generation

Artur Harutyunyan *, Krzysztof Badyda and Łukasz Szablowski

Faculty of Power and Aeronautical Engineering, Institute of Heat Engineering, Warsaw University of Technology, 00-661 Warsaw, Poland; krzysztof.badyda@pw.edu.pl (K.B.); lukasz.szablowski@pw.edu.pl (Ł.S.)
* Correspondence: artur.harutyunyan@pw.edu.pl; Tel.: +48-881531507

Abstract

The increasing penetration of variable renewable energy sources intensifies grid imbalance and challenges the reliability of small-scale power systems. This study addresses these challenges by developing and analyzing a fully integrated hybrid energy system that combines biogas upgrading to biomethane, photovoltaic (PV) generation, hydrogen production via alkaline electrolysis, hydrogen storage, and a gas-steam combined cycle (CCGT). The system is designed to supply uninterrupted electricity to a small municipality of approximately 4500 inhabitants under predominantly self-sufficient operating conditions. The methodology integrates high-resolution, full-year electricity demand and solar resource data with detailed process-based simulations performed using Aspen Plus, Aspen HYSYS, and PVGIS-SARAH3 meteorological inputs. Surplus PV electricity is converted into hydrogen and stored, while upgraded biomethane provides dispatchable backup during periods of low solar availability. The gas-steam combined cycle enables flexible and efficient electricity generation, with hydrogen blending supporting dynamic turbine operation and further reducing fossil fuel dependency. The results indicate that a 10 MW PV installation coupled with a 2.9 MW CCGT unit and a hydrogen storage capacity of 550 kg is sufficient to ensure year-round power balance. During winter months, system operation is sustained entirely by biomethane, while in high-solar periods hydrogen production and storage enhance operational flexibility. Compared to a conventional grid-based electricity supply, the proposed system enables near-complete elimination of operational CO_2 emissions, achieving an annual reduction of approximately 8800 tCO_2, corresponding to a reduction of about 93%. The key novelty of this work lies in the simultaneous and process-level integration of biogas, hydrogen, photovoltaic generation, energy storage, and a gas-steam combined cycle within a single operational framework, an approach that has not been comprehensively addressed in the recent literature. The findings demonstrate that such integrated hybrid systems can provide dispatchable, low-carbon electricity for small communities, offering a scalable pathway toward resilient and decentralized energy systems.

Keywords: hydrogen; biogas; electrolyser; PV; gas turbines; renewable energy; energy storage; gas-steam systems; Aspen HYSYS/PLUS

Check for updates

Academic Editor: Mahmoud Bourouis

Received: 8 December 2025
Revised: 7 January 2026
Accepted: 10 January 2026
Published: 13 January 2026

Copyright: © 2026 by the authors. Licensee MDPI, Basel, Switzerland. This article is an open access article distributed under the terms and conditions of the Creative Commons Attribution (CC BY) license.

1. Introduction

The global energy sector is undergoing a profound transformation driven by decarbonization targets established under the Paris Agreement. The increasing penetration of variable renewable energy sources, such as solar and wind, introduces operational

challenges related to intermittency, grid imbalance, and system reliability-particularly for small-scale and decentralized energy systems. In this context, integrated hybrid energy systems combining multiple renewable and low-carbon energy vectors are increasingly recognized as a key pathway to achieving both environmental sustainability and operational flexibility.

This paper presents a novel configuration of a hybrid energy system that synergistically integrates biogas upgrading to biomethane, photovoltaic (PV) generation, hydrogen production and storage, and a gas-steam combined cycle (CCGT). By coupling renewable electricity generation with chemical energy conversion and dispatchable power production, the proposed system aims to enhance efficiency, improve dispatchability, and support grid stability, making it a promising solution for future sustainable power generation in small municipalities.

To establish the technological background, the following subsections review the current state of development of the individual system components-biogas and biomethane, photovoltaic generation, hydrogen production and storage, and gas turbines-highlighting their advantages, limitations, and future development pathways.

1.1. Biogas/Biomethane

As one of the key components of this hybrid energy system, biogas/biomethane is increasingly recognized as essential component in the transition to sustainable energy systems, offering environmental, economic and energy security benefits. This renewable fuel, produced primarily through anaerobic digestion (AD) of organic waste and agricultural residues, support circular economy models and offer a viable alternative to fossil fuels [1–3].

Its main energy component is methane (CH_4) with a concentration ranging from 50 to 75%, while other components include CO_2, water vapor and trace gases. Biogas can be used directly for heat and electricity generation or it can be upgraded to biomethane - a high-purity form (about 98% CH_4) with properties comparable to natural gas-via technologies like pressure swing adsorption, chemical absorption or membrane separation [4].

Europe leads global biogas production, with most of it currently used in the power sector. While biomethane production is still a small portion of total output, it is expected to grow significantly. The IEA forecasts up to 270% increase in global biogas capacity by 2040, with demand for upgraded biomethane also rising sharply [5].

Several studies highlight the significant greenhouse gas (GHG) emission reductions associated with biogas/biomethane use. For instance, emissions can be reduced by up to 70% compared to natural gas and 65% compared to hydrogen, particularly when these fuels are injected into existing gas grids [1]. When full life cycle benefits and co-products—such as digestate used as fertilizer—are considered, biomethane emerges as a clean and sustainable energy source [6,7]

Biogas development also stimulates economic growth and rural revitalization. In Italy biomethane production from municipal waste has proven economically viable under favorable policy conditions and optimal plant sizing [2]. In Poland, industry players like PGNiG and Orlen are increasingly investing in biomethane despite infrastructural and regulatory limitations [8,9].

Technological advancements continue to enhance biogas performance. Process optimization has been shown to significantly improve biomethane yields and profitability. In China, redesigned AD systems have boosted productivity [10] and pretreatment methods—such as biological, thermal and chemical techniques—have increased feedstock degradability [11–13]. Innovations, such as waste heat recovery and integration with hydroponic farming, further enhance system efficiency [13]. Optimizing parameters like substrate

composition, microbial environment and reactor configuration is also crucial to maximizing yield [14].

Upgrading biogas to high-purity biomethane involves the removal of impurities such as hydrogen sulphide (H_2S), carbon dioxide (CO_2) and moisture. When biogas is upgraded to approximately 98% methane, the resulting biomethane closely matches the properties of natural gas, with the calorific value of around 39.7 MJ/m^3. The critical step in this process is CO_2 removal, typically achieved using technologies like pressure swing adsorption, water scrubbing, physical and chemical absorption, high-pressure membrane separation and cryogenic upgrading. Once refined to natural gas standards, biomethane can be used in all conventional natural gas applications [4,15–17].

The environmental and agricultural value of biogas is further reinforced by co-digestion strategies and alkaline pretreatment, which enhance AD efficiency and promote digestate reuse as natural fertilizer [6]. However, key barriers to large-scale deployment remain. High capital and operational costs persist, especially in areas lacking strong policy support [2,9]. While process additives can boost methane yields, their industrial scalability is limited and often cost-prohibitive [18,19].

Feedstock availability and logistics also present challenges. Although organic waste streams are abundant, their geographic dispersion can hinder plant feasibility. Strategic siting using Geographic Information Systems (GIS) has been proposed to address this issue [20].

Institutional factors such as policy and public perception are critical. The success of biomethane in Europe hinges on supportive legal frameworks, public investment and awareness-building efforts [8,9]. Without these enablers, even technologically robust solutions may struggle to scale.

In conclusion, while biogas and biomethane offer documented advantages in GHG reduction, waste valorization and energy diversification, broader adoption demands overcoming persistent economic, technical and policy challenges. Interdisciplinary collaboration, sustained innovation and comprehensive regulatory support will be essential to realizing their full role in the low-carbon future [1,6,13].

1.2. Photovoltaic (PV) Generation

PV technology offers a clean and reliable method of converting solar energy directly into electricity using light-absorbing materials, with advantages such as minimal maintenance, modular scalability and suitability for both small-scale and large-scale installations [21]. However, the performance of PV systems is strongly influenced by environmental factors like solar irradiation and temperature, which complicate accurate energy output forecasting and make modeling under variable climatic conditions essential for efficient system design [22–24]. To address PV intermittency and improve overall system resilience, hybrid configurations combining PV with other energy sources, such as gas turbines or hydrogen storage systems, have been explored. For instance, a hybrid micro gas turbine (MGT)—PV system demonstrated improved energy production and reduced emissions, although it introduced trade-offs such as increased local CO emissions and greater operational complexity [25]. Similarly, a PV-gas turbine-electrolyser hybrid system achieved high efficiency and significant cost and CO_2 reductions for residential applications, though economic sensitivity to natural gas and electrolyser prices remains a challenge [26].

Expanding on hybrid concepts, the integration of PV systems with hydrogen storage and fuel cells in microgrids has shown potential for deep decarbonization, particularly where land availability limits PV expansion [27]. In such setups, hydrogen can serve as a long-duration storage medium, as seen in a theoretical 100 MW hybrid plant using hydrogen-fuelled turbines, which achieved significant lifecycle CO_2 savings despite

relatively high electricity production costs [28]. Life-cycle assessments confirm that the environmental impact of hydrogen production via PV-powered electrolysis varies widely, largely due to methodological inconsistencies and the carbon intensity of electricity inputs, underscoring the need for standardization in sustainability evaluation [29].

Hydrogen-based storage, when paired with batteries in off-grid microgrids, has proven to be the most cost-effective and autonomous solution, especially for remote communities aiming for 100% renewable energy coverage [30]. Furthermore, systems that participate in multiple energy markets—electricity, natural gas and hydrogen—can enhance profitability through strategic arbitrage, though success depends heavily on market structure and participation rules [31]. Other grid-connected setups, such as PV-trigeneration systems with hydrogen output, show both economic viability and notable GHG reductions, particularly when integrated into institutional or campus energy infrastructures [32].

Moreover, multi-objective optimization of PV/battery/hydrogen systems offers resilience against demand fluctuations and supports emerging economic models, such as trading surplus power for green certificates, enhancing financial and environmental performance [33]. Integrated energy systems that employ both battery and hydrogen storage benefit from coordinated operation, improving self-sufficiency and reducing power abandonment, although they still face issues like energy loss and increased emissions if not properly managed [34,35]. Thus, while PV and PV-hydrogen hybrid technologies offer significant promise for low-carbon energy transitions, realizing their full potential requires overcoming economic, technical and regulatory challenges through optimized system design, advanced forecasting and supportive policy frameworks.

1.3. Hydrogen

Another important component of this hybrid energy system is hydrogen, widely recognized as a clean, high-energy fuel with the potential to decarbonize multiple sectors, including industry, mobility and power generation. Its significance lies not only in its regenerative and eco-friendly nature but also in its ability to serve as a flexible energy carrier that supports the integration of intermittent renewable energy sources.

China is currently the world's largest hydrogen producer, the position it has maintained for several years. Due to prevailing economic conditions, approximately 95% of the country's hydrogen is derived from fossil fuel sources such as coal and natural gas [36]. This fossil-based production poses a significant challenge to the development of green hydrogen, which relies on renewable energy and sustainable technologies.

A promising alternative is hydrogen production via water electrolysis, which splits water molecules into hydrogen and oxygen using electricity. Several electrolysis technologies exist, each at different stages of technological maturity. The most established is alkaline electrolysis (AEL), which operates at low temperatures (70–90 °C) and has been in use for decades due to its low cost and system durability [37,38]. However, AEL systems suffer from limitations such as low current densities, gas crossover and limited dynamic response [39].

Proton exchange membrane (PEM) electrolysers are another commercially available option. They offer high current density, rapid response and high-purity hydrogen, making them suitable for fluctuating energy sources like solar and wind [39,40]. However, PEM systems are more expensive due to the use of noble metals and complex membrane materials and they have shorter lifespans in acidic environments.

In contrast, solid oxide electrolyser cells (SOEC) operate at high temperatures (650–850 °C), offering very high theoretical efficiencies and the ability to use industrial-grade heat. These systems can reduce electricity consumption by utilizing thermal energy, but they remain in the laboratory phase, facing technical challenges such as material degradation under extreme conditions [38].

A newer and still experimental method, anion exchange membrane (AEM) electrolysis, aims to combine the best features of AEL and PEM by using inexpensive materials while achieving higher performance. However, more research is needed to improve the durability and efficiency of AEM systems [38,39].

Operational parameters also significantly affect the efficiency of electrolysis. A temperature of 80 °C was identified as optimal for minimizing power consumption in alkaline electrolysers [40]. Process modeling has shown that increasing the temperature while reducing pressure enhances system performance [41]. Thermodynamic and kinetic analyses reveal several resistive losses in electrolysis, including activation resistance, ionic resistance, gas bubble formation and electric circuit losses [40,42]. Cost forecasts are promising, with green hydrogen expected to drop from €3.70/kg to €2.00/kg by 2040, potentially reaching cost parity with fossil-derived hydrogen. However, concerns persist regarding the reliance on scarce materials, such as iridium in proton exchange membrane (PEM) systems and the environmental implications of large-scale deployment [43].

1.4. Hydrogen Energy Storage

The next key component of the hybrid energy system is the hydrogen energy system. Hydrogen, the lightest element, has a high energy content per unit mass (141.86 MJ/kg), which often leads to the perception that it is a superior fuel compared to natural gas. However, its extremely low density results in the very low volumetric energy density, posing significant challenges for storage and transportation. These physical characteristics directly impact its role in the energy system. Hydrogen storage, therefore, becomes a critical pillar in building a viable hydrogen economy. Despite being a clean, energy-dense carrier by weight, hydrogen's low critical temperature and volumetric density present significant storage challenges [44]. Current storage technologies include high-pressure cylinders, cryogenic tanks and solid-state storage systems, with high-pressure gas storage being the most commercially mature option. These include vessel types from fully metallic to polymer composite tanks [45].

Material-based storage systems, such as those using metal hydrides and carbon nanomaterials, are gaining traction for their high gravimetric capacity and improved safety. Magnesium-based hydrides, for example, show promise despite their high desorption temperatures [46]. These materials offer better stability and lower degradation rates, although they still suffer from relatively low volumetric energy density even at high pressures [47].

Several major hydrogen storage projects have been launched globally, emphasizing the increasing role of hydrogen in the clean energy transition. In Germany, the HyCAVmobil project is developing an underground hydrogen storage cavern in Rüdersdorf, demonstrating large-scale, demand-responsive green hydrogen storage [48]. The DESSERT project, initiated by the European Union in July 2024, is advancing sustainable hydrogen storage technologies, particularly focusing on underground storage formations [49]. Additionally, the Clean Hydrogen Joint Undertaking has funded 31 new projects across 28 countries, many of which incorporate hydrogen storage solutions to strengthen the hydrogen value chain [50].

As these projects advance, geological storage presents a promising solution for long-term, seasonal or large-scale hydrogen storage. Underground hydrogen storage (UHS) in depleted gas fields, aquifers or salt caverns could provide scalable options, although site-specific assessments are necessary to mitigate risks such as leakage or material reactivity. International projects like Roads2HyCOM and H2STORE are exploring the technical, microbial and geochemical challenges of UHS, underscoring the importance of global collaboration and continued innovation in realizing a hydrogen-powered energy future [51,52].

1.5. Gas Turbine

Hydrogen-powered gas turbines are emerging as a critical component in the transition toward low-carbon energy systems. Hydrogen, due to its high energy content and zero-carbon combustion, offers significant potential in reducing greenhouse gas emissions when integrated into gas turbine technology [53–55]. However, its adoption presents technical challenges, including flame stability, flashback and increased nitrogen oxide (NOx) emissions [56–58].

Industrial advancements have focused on overcoming these challenges through innovations in combustor design and fuel flexibility. Companies like GE and Mitsubishi are developing combustors compatible with hydrogen and ammonia, utilizing technologies such as micro-mixing, aerodynamic flame stabilization, and sequential combustion to manage emissions and improve efficiency [56,59,60]. Combustion strategies continue to evolve, with research highlighting the trade-offs between diffusive and lean premixed flame designs—lean premixed systems offer superior efficiency with hydrogen but are more sensitive to pressure drops and temperature limits [61].

Hydrogen's integration into hybrid renewable energy systems also supports grid stability and decarbonization. Studies have demonstrated that hybrid systems, which combine photovoltaic energy, battery banks and gas turbines powered by hydrogen or hydrogen blends, can significantly reduce lifecycle costs and emissions [62,63].

Micro gas turbines (MGTs) represent another promising application. Their fuel flexibility, compact design and potential for decentralized power generation make them ideal for integration with renewable energy sources like solar fields and fuel cells [64,65]. Redesigning MGTs to operate with hydrogen or hydrogen-methane blends has shown promising results, with stable combustion and near-zero CO_2 emissions achieved even at high hydrogen concentrations [66,67].

Economic analyses reinforce hydrogen's promise in gas turbines. For example, the addition of hydrogen (up to 20%) to natural gas in conventional turbines results in fuel savings and efficiency gains, although higher concentrations necessitate substantial system upgrades [68]. In combined-cycle systems, hydrogen improves operational flexibility and reduces CO_2 emissions, particularly when integrated with hydrogen storage and fuel cells [69,70]. Exergo-economic studies of advanced cogeneration systems further confirm hydrogen's role in reducing energy costs while producing steam and electricity efficiently [71].

On a larger scale, hydrogen-fired turbines offer a strategic advantage in national energy planning. Techno-economic models across 15 European countries project that hydrogen turbines will become increasingly competitive post-2040, particularly under strict CO_2 caps, by providing flexible, dispatchable power [72]. Nevertheless, cost barriers remain, primarily due to the high expense of hydrogen production via electrolysis or steam methane reforming [54,56].

Hybrid models simulating the integration of hydrogen and renewable energy systems predict notable improvements in emissions reduction and system sustainability. Adding hydrogen to methane in gas turbines enables leaner combustion, modest efficiency gains and high performance even with less efficient turbomachinery by lowering the fuel's flammability limit and mitigating system constraints [73].

Despite the technical and economic hurdles, continued research and development, supported by regulatory frameworks and industrial investment, are accelerating the viability of hydrogen-powered gas turbines. These systems will be pivotal in achieving the 2050 global decarbonization targets [53,56].

1.6. Research Gap and Contributions

Despite extensive research on individual components such as biomethane, photovoltaic generation, hydrogen production, energy storage, and gas turbines, existing studies predominantly investigate these technologies either in isolation or in limited hybrid configurations. Most recent works focus on PV-battery-hydrogen systems or PV-assisted gas turbines, while the simultaneous integration of biogas upgrading, hydrogen production and storage, photovoltaic generation, and a gas-steam combined cycle within a single operational framework remains largely unexplored. Moreover, many studies emphasize optimization or economic indicators without providing a detailed, process-based representation of physical system interactions under full-year operation.

This study addresses these gaps by proposing and analyzing a fully integrated hybrid biogas–hydrogen–PV–energy storage–gas turbine system using high-resolution temporal data and detailed thermodynamic modeling. The main contributions of this work are:

- the development of a comprehensive process-based simulation framework linking renewable electricity generation, chemical energy conversion, storage, and dispatchable power production;
- the evaluation of year-round operational feasibility for a small municipality under realistic hourly and seasonal variability;
- the demonstration of biomethane-supported operation during low-solar winter periods; and
- the identification of technical and regulatory challenges affecting system scalability and real-world deployment.

1.7. State-of-the-Art Comparison

To contextualize the novelty of the proposed approach, Table 1 compares recent state-of-the-art hybrid renewable energy system studies published since 2021 with the system investigated in this work.

Table 1. Comparison of recent state-of-the-art hybrid renewable energy system studies (2021–2025).

Ref.	Year	Study Region	Optimization/ Method	System Configuration	Financial Viability Metrics	Main Results	Limitations
[27]	2023	USA	Techno-economic simulation	PV + Gas Turbine + Hydrogen + Battery	LCOE, CO_2 emissions	Hydrogen enables deep decarbonization of PV-GT microgrid	High hydrogen infrastructure cost
[31]	2022	EU	Linear optimization	PV + Battery + Hydrogen	LCOH, Market revenues	Multi-market operation significantly reduces hydrogen cost	Market-dependent feasibility
[32]	2022	Turkey	Techno-economic analysis	PV + Trigeneration + Hydrogen	NPV, IRR, Payback	Economically viable campus-scale system	Limited scalability
[33]	2023	China	Robust optimization (NSGA-II)	PV + Battery + Hydrogen	LCOE, Carbon credits	Improved resilience under uncertainty	Increased system complexity
[34]	2024	China	Two-stage optimization	PV + Battery + Hydrogen	Energy autonomy, system cost	Reduced curtailment and higher self-consumption	Requires advanced control

Table 1. *Cont.*

Ref.	Year	Study Region	Optimization/ Method	System Configuration	Financial Viability Metrics	Main Results	Limitations
[35]	2024	China	Dynamic optimization	PV + Battery + Hydrogen community	Carbon neutrality indicators	Supports carbon-neutral communities	Aging-related losses
[64]	2023	China	MILP optimization	Renewable sources + Gas Turbine + Storage	System cost, emissions	Improved reliability and flexibility	Partial fuel decarbonization
[72]	2024	China	Exergy & exergoeco-nomic analysis	Hybrid RES + Hydrogen Fuel Cells	Exergy cost, efficiency	Reduced exergy destruction and emissions	High modeling complexity
This work	2025	Poland	Process-based simulation (Aspen Plus & HYSYS)	Biogas + Biomethane + PV + Hydrogen (Electrolysis & Storage) + Gas-Steam Combined Cycle	Energy autonomy, efficiency, grid flexibility	Year-round dispatchable supply; winter operation fully supported by biomethane	Hydrogen cost, regulatory gaps, idealized operation

Abbreviations: LCOE—Levelized Cost of Electricity; LCOH—Levelized Cost of Hydrogen; NPV—Net Present Value; IRR—Internal Rate of Return; NSGA-II—Non-dominated Sorting Genetic Algorithm II.

1.8. Synthesis of State-of-the-Art Comparison

As shown in Table 1, existing studies predominantly focus on partial hybrid configurations, typically combining photovoltaic generation with batteries, hydrogen storage, or gas turbines. In contrast, the present study provides a process-level, fully integrated analysis of a hybrid system that simultaneously couples biogas upgrading, hydrogen production and storage, photovoltaic generation, and gas-steam combined-cycle power generation. This integrated approach enables high dispatchability and deep operational decarbonization for small, predominantly self-sufficient communities.

1.9. Roadmap of the Paper

The remainder of this paper is organized as follows. Section 2 defines the main scope of the work and discusses open issues related to integrated renewable hybrid energy systems. Section 3 describes the proposed system configuration and the associated modeling framework. Section 4 presents the simulation results and performance analysis, including energy balance and CO_2 emissions reduction. Finally, Section 5 summarizes the key findings, discusses the limitations of the study, and outlines directions for future research.

2. Main Scope of the Work and Open Issues in the Context of Renewable Hybrid Energy Systems

As highlighted in the recent literature, extensive research has been conducted on individual components of renewable hybrid energy systems, including biogas and biomethane, photovoltaic (PV) generation, hydrogen production and storage, and gas turbines. However, most existing studies investigate these technologies either in isolation or in simplified hybrid configurations involving only two or three components. Comprehensive analyses addressing the simultaneous integration of biogas upgrading, hydrogen production and storage, photovoltaic generation, and gas-steam combined-cycle power generation remain limited, particularly for small-scale, community-level applications.

2.1. Scope and Objectives of the Study

The primary objective of this work is to analyze the operational feasibility and performance of a fully integrated hybrid biogas–hydrogen–PV–energy storage–gas turbine system designed to supply electricity to a small municipality. Rather than focusing on system sizing optimization or purely economic indicators, the study emphasizes system-level integration, dispatchability, and year-round operational balance under realistic hourly and seasonal variability.

The specific objectives of the study are to:

- assess the ability of the proposed hybrid system to meet electricity demand on an hourly basis throughout the year;
- evaluate the interaction between renewable electricity generation, hydrogen production and storage and dispatchable power generation;
- analyze the role of biomethane in ensuring system reliability during low-solar winter periods;
- quantify the operational CO_2 emission reduction relative to a conventional grid-based electricity supply.

2.2. Performance Metrics and Evaluation Criteria

To address these objectives, system performance is evaluated using the following metrics:

- energy balance and self-sufficiency, expressed as the ability to meet demand without grid imports;
- dispatchability and operational flexibility, assessed through the ability of the gas-steam combined cycle to respond to demand and renewable variability;
- hydrogen utilization efficiency, including hydrogen production, storage, and blending in the gas turbine;
- operational CO_2 emissions reduction, quantified relative to the Polish electricity grid.

These metrics are selected to reflect the operational performance of the system rather than economic optimization outcomes.

2.3. System Boundaries and Assumptions

The analysis is conducted within defined system boundaries. The proposed hybrid system is assumed to operate under idealized conditions, with continuous availability of system components, stable market conditions, and reliable communication and control infrastructure. Equipment degradation, unexpected outages, and dynamic price fluctuations are not explicitly modeled and are instead discussed as limitations of the study.

The system is modeled as grid-connected but predominantly self-sufficient, allowing limited interaction with the external grid to enhance operational flexibility while prioritizing local renewable energy utilization.

2.4. Open Issues and Challenges

Despite the promising performance of integrated hybrid systems, several open issues remain. These include:

- regulatory and market barriers affecting hydrogen production, storage, and grid interaction;
- high capital costs associated with electrolyzers and hydrogen storage infrastructure;
- uncertainties related to long-term hydrogen storage performance and safety;
- the need for advanced control strategies to manage multi-energy vector interactions under real-world operating conditions.

Addressing these challenges is essential for large-scale deployment and commercialization of integrated hybrid energy systems.

2.5. Broader Applicability of the Case Study

Although the proposed system is analyzed for a specific location in Poland, the system architecture and modeling approach are transferable to other regions with access to renewable resources and biomass feedstock. The study therefore provides generalizable insights into the design and operation of hybrid renewable energy systems for small communities, rather than a site-specific optimization.

3. The Description of the Model

3.1. Case Study Definition and System Overview

The proposed hybrid energy system is designed to provide uninterrupted electricity supply throughout the year, under day-and-night operating conditions, to a small settlement of approximately 4500 inhabitants. The system architecture aims to ensure a high degree of energy autonomy while maintaining operational flexibility through the integration of renewable generation, energy storage, and dispatchable power conversion technologies.

The selected case study location is situated in central-northern Poland, approximately 80–90 km northwest of Warsaw, as illustrated in Figure 1.

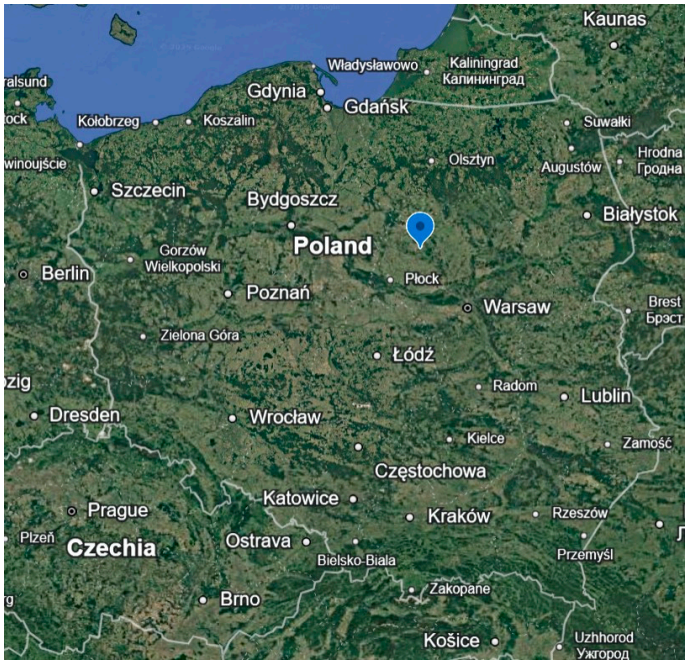

Figure 1. Geographical location of the selected case study area in Poland (approximately 80–90 km northwest of Warsaw), used for the assessment of the integrated biogas–hydrogen–photovoltaic–energy storage–gas turbine system.

The selected area includes settlements with populations close to the target scale of the proposed system and is characterized by intensive agricultural activity, enabling a sustainable and locally available biomass supply for biogas production. At the same time, the region exhibits solar irradiation levels representative of Central European climatic conditions, making it suitable for assessing photovoltaic-based hybrid energy systems for small municipalities.

An additional motivation for selecting this location is the presence of existing agro-industrial renewable energy infrastructure, which enables evaluation of the proposed hybrid system under realistic operational conditions. The site includes a sugar processing plant equipped with an agricultural biogas installation with an electrical capacity of ap-

proximately 2 MW, as well as a photovoltaic (PV) installation with an installed capacity of about 3 MW. According to the plant's medium-term development strategy, the PV capacity is planned to be expanded to 10 MW or more, which is consistent with the assumptions adopted in this study and reflects realistic future expansion pathways.

At present, the biogas plant primarily utilizes sugar beet pulp as its main substrate, supplemented by additional agricultural feedstocks. However, the long-term operational strategy of the plant foresees a gradual reduction or complete phase-out of sugar beet pulp as a biogas substrate due to its increasing economic value as dried animal feed. Consequently, alternative substrates—namely corn silage, shredded straw, and rapeseed pomace—are expected to play a dominant role in future biogas production. These substrates were therefore selected for the present analysis to represent anticipated future operating conditions rather than the current transitional state.

Although the system is analyzed for a specific location in Poland, the methodological framework, modeling approach, and system configuration are transferable to other regions with comparable biomass availability and solar resource profiles. As such, the results are relevant for a wide range of rural and semi-urban communities seeking low-carbon, locally integrated energy solutions.

The principal schematic of the proposed hybrid energy system is presented in Figure 2.

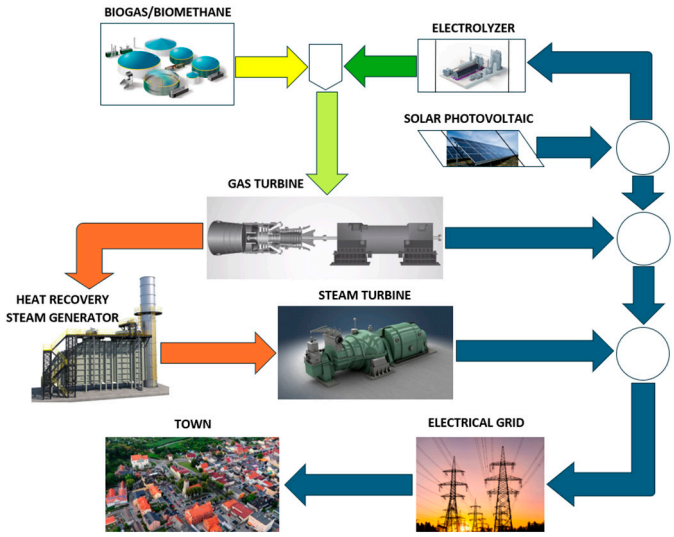

Figure 2. Principal schematic of the integrated biogas–hydrogen–photovoltaic–energy storage–gas–steam combined-cycle hybrid energy system. Yellow arrows represent biogas/biomethane flows, green arrows hydrogen flows, and light-green arrows their mixture supplied to the gas turbine. Blue arrows denote electrical energy flows, while red arrows indicate thermal (heat) energy.

3.2. Operational Concept of the Hybrid Energy System

In the proposed hybrid energy system, raw biogas is produced from locally available agricultural feedstocks through an anaerobic digestion (AD) process. The resulting biogas is subsequently treated to remove undesired components, such as carbon dioxide, hydrogen sulfide, and moisture, and upgraded to biomethane. The upgraded biomethane serves as the primary dispatchable fuel for the gas turbine combustion chamber, enabling reliable electricity generation independent of solar resource availability.

The system further integrates a photovoltaic (PV) installation, which supplies electricity directly to meet the settlement's demand during periods of sufficient solar irradiation. When PV generation exceeds instantaneous electricity demand, the surplus electrical energy is diverted to an alkaline water electrolyzer, where it is utilized for green hydrogen produc-

tion via water electrolysis. This operational strategy allows excess renewable electricity to be converted into a storable chemical energy carrier rather than being curtailed.

The produced hydrogen is stored and subsequently supplied to the gas turbine combustion chamber, where it is co-fired with biomethane. Hydrogen blending enhances fuel flexibility, supports low-load operation, and contributes to the reduction of carbon-based fuel consumption, thereby lowering operational CO_2 emissions while maintaining stable turbine performance.

The gas turbine operates as part of a gas-steam combined-cycle configuration, integrated with a condensation-type steam turbine through a heat recovery system. This configuration increases the overall electrical efficiency by recovering waste heat from the gas turbine exhaust for additional power generation in the steam cycle.

To further enhance operational flexibility and system stability, the hybrid energy system is assumed to be connected to the external electrical grid, allowing short-term power exchange to mitigate transient mismatches between electricity generation and demand and to support secure operation under variable renewable generation conditions. The overall operational concept and main energy flows of the hybrid system follow the configuration illustrated in Figure 2.

3.3. Meteorological Data and Boundary Conditions

The photovoltaic energy yield and hydrogen production simulations were based on full-year, high-resolution meteorological data for the year 2023, obtained from the EU Photovoltaic Geographical Information System (PVGIS). The PVGIS-SARAH3 satellite-based solar radiation database was selected, as it provides validated hourly data with high spatial and temporal resolution for Europe, ensuring a reliable representation of local climatic conditions.

The meteorological inputs include ambient temperature, global horizontal irradiation (GHI), direct normal irradiation (DNI), and the diffuse-to-global irradiance ratio, which are critical parameters for accurately modeling photovoltaic system performance and electrolysis operation. These data were extracted for the geographical coordinates of the selected case study location defined in Section 3.1.

Figure 3 presents the monthly average ambient temperature and the diffuse-to-global irradiance ratio for the selected location in 2023. The data show a pronounced seasonal temperature variation typical of Central European climates, with average ambient temperatures ranging from approximately 1–2 °C in winter months to above 20 °C during summer. This temperature variation directly influences photovoltaic module efficiency and system losses and was explicitly accounted for in the PV performance model.

The diffuse-to-global irradiance ratio increases notably during autumn and winter months, reflecting higher cloud coverage and reduced direct solar radiation. This characteristic is particularly important for accurate PV modeling, as it affects both total energy yield and the relative contribution of diffuse radiation under low-irradiance conditions.

Figure 4 illustrates the monthly distribution of horizontal irradiation and direct normal irradiation for 2023. Peak solar irradiation occurs between May and July, while minimum values are observed during the winter period from November to January. This pronounced seasonal imbalance highlights the necessity of integrating long-term energy storage and dispatchable power generation technologies to ensure year-round electricity supply.

The meteorological data were applied consistently across all relevant subsystems of the hybrid energy model. Specifically, the hourly solar irradiation and temperature data were used as inputs for the photovoltaic power generation model, while the resulting PV electricity profiles were subsequently used to define the electrolyzer operating schedule and hydrogen production potential. This approach ensures that the influence of both seasonal

and diurnal variability in solar resource availability is fully captured in the annual energy balance analysis.

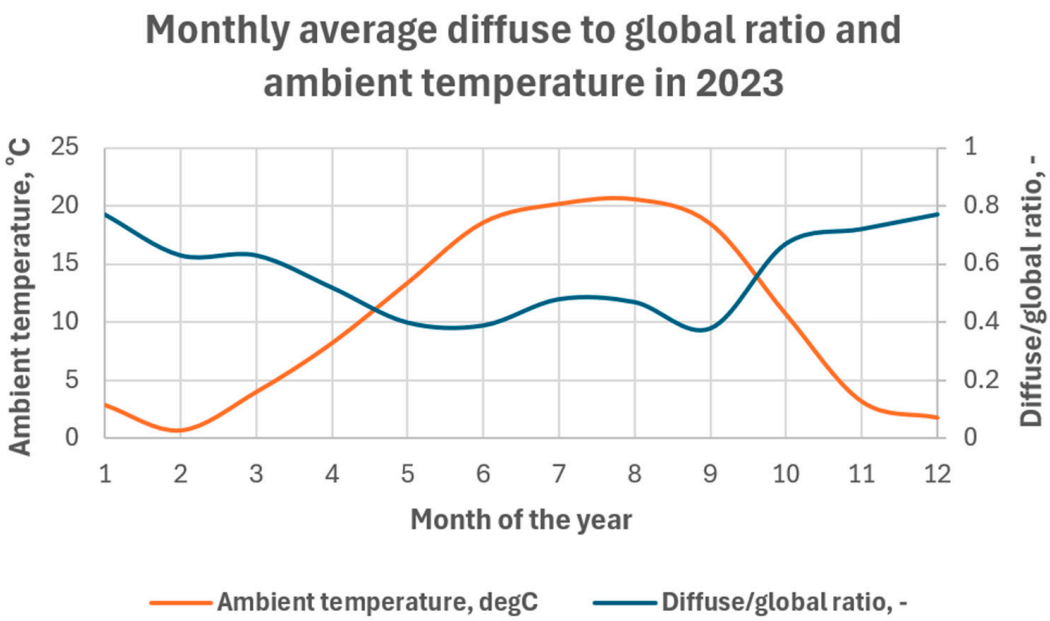

Figure 3. Monthly average diffuse to global ratio and ambient temperature in 2023.

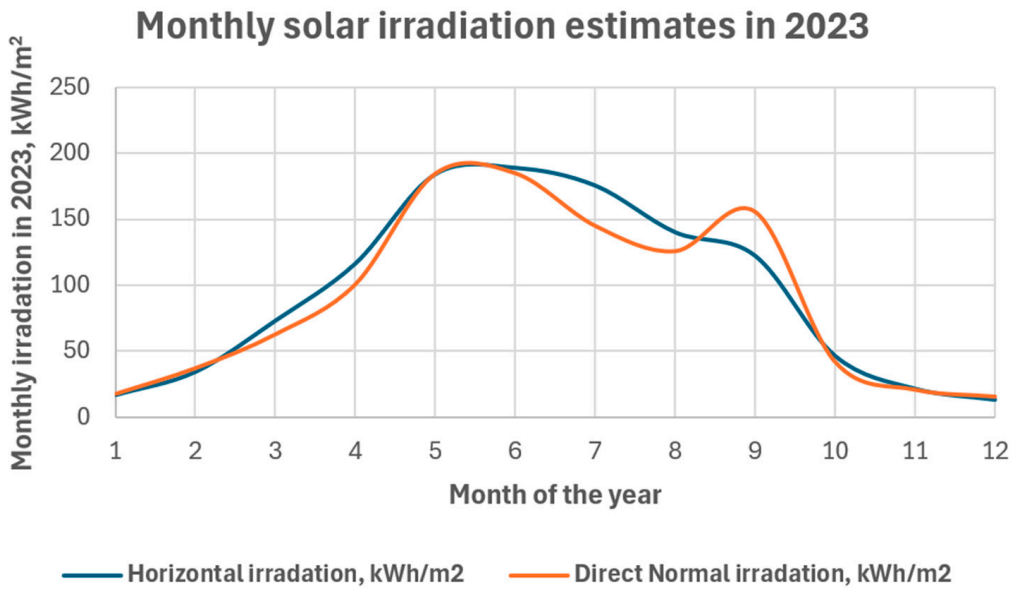

Figure 4. Monthly solar irradiation estimates in 2023.

The use of measured satellite-based hourly meteorological data, rather than synthetic or averaged weather profiles, improves the realism and credibility of the simulation results. It enables a more accurate assessment of system performance under realistic operating conditions, particularly with respect to renewable energy intermittency, surplus electricity availability, and the role of hydrogen as a long-duration energy storage medium.

3.4. Biogas Plant

The biogas plant operates using three types of feedstock as substrates: corn silage, shredded straw and rapeseed pomace. As mentioned above, these feedstocks were selected based on their availability in the local area.

Table 2 presents the annual quantities, dry matter content, organic content in dry matter and—based on reference data—the average biogas and biomethane yields for each feedstock [74].

Table 2. Mass balance of feedstock in biogas plant.

	Feedstock	Quantity	Dry Matter Content	Organic Content in Dry Matter	Biogas Yield Average	CH_4 Yield Average
	Unit	t/Year	%	%	Nm^3/t of Feedstock	%
1.	Corn silage	8000	32	93	198	55
2.	Shredded straw	8000	75	88	260	55
3.	Rapeseed pomace	6000	92	87	630	48
	TOTAL	22,000	64	89	338	51

Table 3 provides the calculated values for total annual biogas production, the corresponding biomethane yield and the equivalent electrical energy output.

Table 3. Energy balance of feedstock in biogas plant.

	Feedstock	Biogas Production	Biomethane Yield		Electrical Output (If Cogeneration Is Used)
	Unit	Nm^3/Year	Nm^3/Year	MWh in Fuel/Year	kWh
1.	Corn silage	1,584,000	884,535	8622	415
2.	Shredded straw	2,080,000	1,161,510	11,322	545
3.	Rapeseed pomace	3,780,000	1,842,171	17,957	865
	TOTAL	7,444,000	3,888,216	37,901	1825

From the selected feedstock mix—amounting to approximately 22,000 t annually—around 740,000 Nm^3 of biogas can be produced, based on the following formula:

$$\text{Biogas production} = \text{Feedstock quantity} \times \text{Average biogas yield} \quad (1)$$

Of this, approximately 3,888,000 Nm^3 is pure biomethane. When used for electricity generation at an efficiency of around 40%, this can yield a continuous electrical output of approximately 1825 kWh.

The produced biomethane quantity was calculated according to the below provided formula:

$$\text{Biomethane production} = (100\% - 0.5\%) \times (\text{Biogas production}/98\%) \quad (2)$$

where

0.5% represents biogas losses and

98% is the efficiency of biomethane upgrading plant.

3.5. Photovoltaic Installation

The photovoltaic (PV) installation is modeled for the same geographical location as the biogas plant and hybrid energy system described in Section 3.1, with coordinates 52°49′51.6″ N, 20°14′34.8″ E. Co-location of the PV installation with existing agro-industrial

infrastructure enables efficient coupling with biogas production and hydrogen generation and reflects realistic deployment conditions for integrated rural energy systems.

Photovoltaic electricity generation is simulated using hourly meteorological data for the year 2023 obtained from the PVGIS-SARAH3 database, as described in Section 3.3. The PV system is assumed to be grid-connected, allowing power exchange with the external electrical grid when necessary.

The selected PV technology consists of crystalline silicon photovoltaic modules, chosen due to their high efficiency, technological maturity, and widespread commercial deployment. The total installed peak capacity of the PV system is 10 MW. Overall system losses are assumed to be 14%, accounting for temperature effects, inverter inefficiencies, cabling losses, and module soiling.

A fixed, free-standing mounting structure is assumed for the PV installation. The modules are installed with a tilt angle of 35° and an azimuth angle of 0°, corresponding to a true south orientation, which is optimal for maximizing annual energy yield at the selected latitude.

The simulated hourly power output profile of the PV system for the entire year of 2023 is shown in Figure 5. This power profile forms the basis for the electricity balance calculations and determines the availability of surplus renewable electricity for hydrogen production via electrolysis.

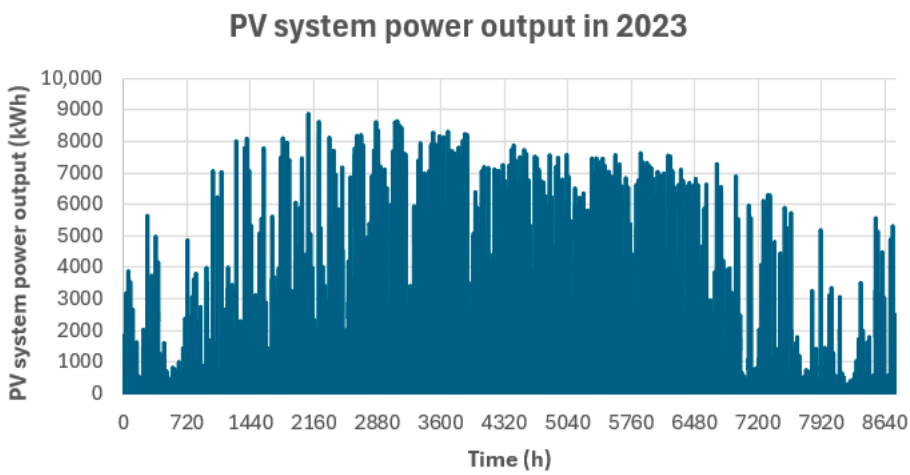

Figure 5. Hourly photovoltaic power output of the 10 MW PV system at the selected location for the year 2023.

3.6. Alkaline Water Electrolyzer for Hydrogen Production

The electrolysis process was modeled using the commercial simulation software Aspen Plus. In the simulation, potassium hydroxide (KOH) was used as an input component mixed with water to enhance conductivity during electrolysis. The key chemical reactions involved are:

$$H_2O \rightleftharpoons OH^- + H^+$$

$$\mathrm{KOH} \rightleftharpoons OH^- + K^+$$

Before simulating the electrolysis reaction, several important parameters were defined, including the cell voltage, the power requirement of the electrolyzer and the conversion rate of water into hydrogen gas [38].

Water and potassium hydroxide are supplied to the system. This mixture is first pressurized to 27 bar using a pump. After pressurization, the stream is heated by a heater before entering the conversion reactor. Within the conversion reactor, the water conversion

rate is set at 5% and the power requirement for the electrolysis process is specified at 230 kW.

The conversion reaction produces two output streams: vapor and liquid. The vapor stream is directed to a component splitter (Splitter-1), where it is separated into hydrogen and oxygen. Simultaneously, the liquid stream is sent to another splitter (Splitter-2), where oxygen is separated from water. The remaining water is then recycled back into the process to improve efficiency and reduce waste. The schematic diagram of the electrolyzer system is illustrated in Figure 6.

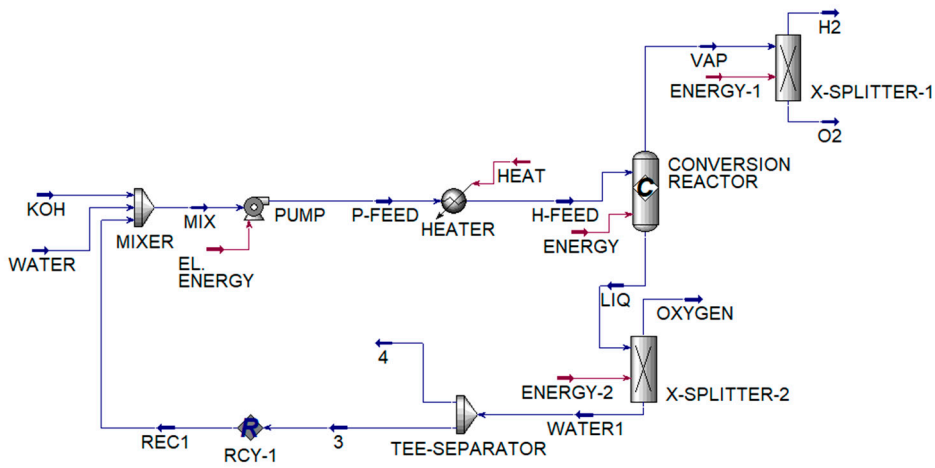

Figure 6. The schematic diagram of the modeled alkaline water electrolyser system. Blue lines denote material streams, while red lines represent energy streams (heat or electrical power).

Figure 7 shows the relationship between the required electrical power input (kWh) and the resulting hydrogen production and water consumption mass flow rates (kg/s), as determined by the simulation model of the system.

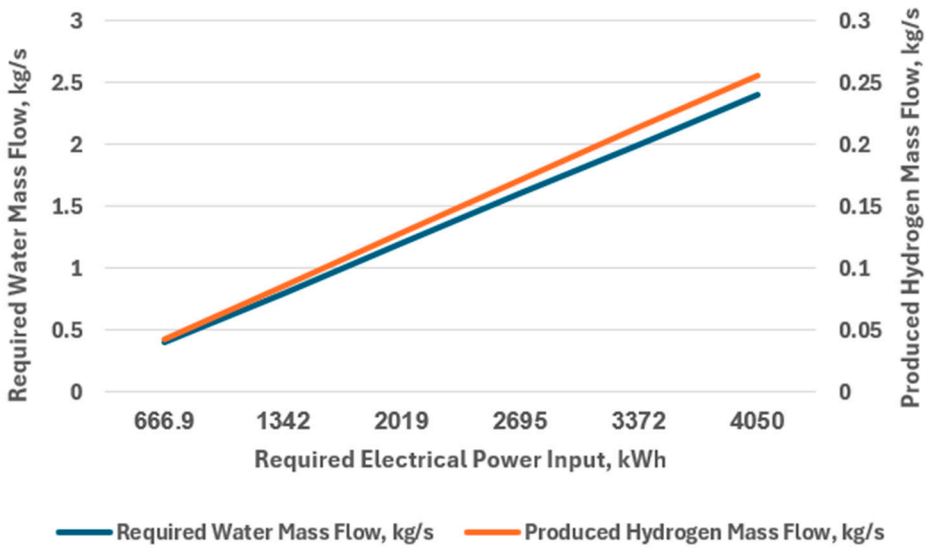

Figure 7. Required water and produced hydrogen mass flow rates at different electrical power input levels for the electrolysis system.

3.7. Gas-Steam Combined Cycle

For the modeling and simulation of the gas-steam combined cycle, the Aspen HYSYS software was selected as the primary calculation tool. The air parameters were assumed according to ISO standard conditions, with the temperature of 15 °C and the pressure of 1.013 bar.

In this model, the Kawasaki GPB-17D gas turbine was selected as the core component of the gas-steam combined system, along with a corresponding steam turbine appropriately sized for integration with the gas turbine. Table 4 presents the technical specifications of the selected equipment. The gas turbine data, provided by the manufacturer, apply to both 100% methane and 100% hydrogen fuel conditions.

Table 4. Kawasaki gas turbine technical data.

Kawasaki GPB-17D Gas Turbine Technical Data		
Fuel type	Methane	Hydrogen
Power output	1817 kW(e)	1902 kW(e)
Efficiency	27.2%	27.5%
Pressure ratio	18.0:1	18.0:1
Exhaust mass flow	7.99 kg/s	7.89 kg/s
Exhaust temperature	528 °C	528 °C
NOx reduction method	Water inject.	Water inject.
Steam turbine and steam boiler technical data		
Power output		1060 kW(e)
Live steam pressure		36 bar(a)
Live steam temperature		520 °C
Steam mass flow		1.0 kg/s
Exhaust gas temperature		149 °C

The main process flow diagram of the modeled gas-steam combined system is shown in Figure 8.

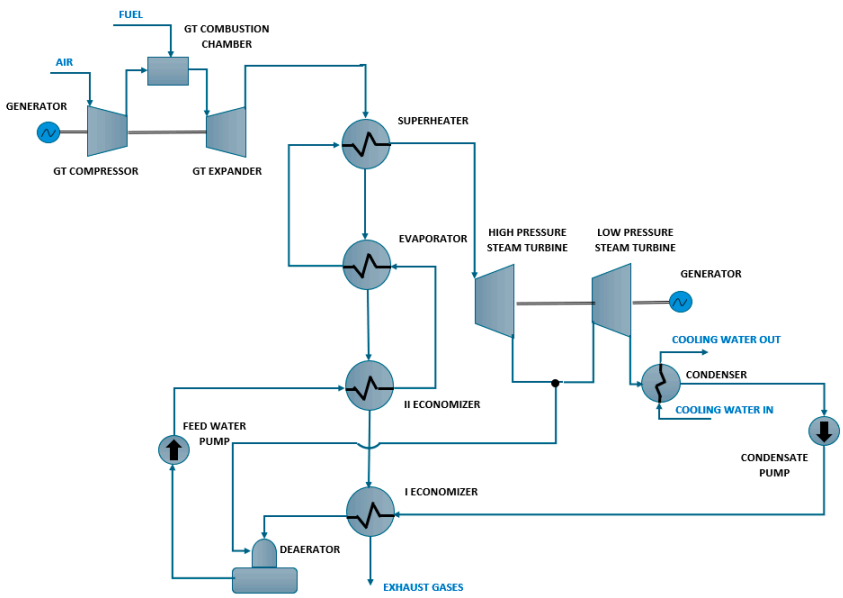

Figure 8. The schematic diagram of the modeled CCGT power plant [75].

The installation consists of the following components:

- Gas turbine section, including the compressor, combustion chamber and expander
- Heat recovery system, incorporating two-stage economizers, an evaporator and a superheater

- Steam turbine section, comprising high-pressure (HP) and low-pressure (LP) turbines
- Additional components of the steam cycle, including the condenser, deaerator and pumps for both condensate and feedwater

The design of the gas turbine's centrifugal air compressor was based on efficiency and polytropic head calculations. For this purpose, the Schultz Polytropic Method was applied [76], which assumes an idealized polytropic compression path from the inlet to the discharge conditions. This method offers a simplified yet reliable approach for modeling compressor performance.

The gas turbine expander was modeled separately, with an isentropic efficiency of 85.35% defined as the primary performance parameter. This allowed evaluation of expansion characteristics under various thermodynamic scenarios.

The combustion chamber was developed using a reactor model based on Gibbs Reactions Method. This approach is particularly suitable for simulating combustion processes involving multi-component gaseous fuels.

To maintain a stable Temperature After Turbine (TAT) in the cycle, an Adjust function was incorporated into the model. This control mechanism allowed the TAT to be regulated at approximately 528 °C, depending on variations in fuel type or mass flow rate within the combustion chamber.

For a more accurate representation of the steam turbine (ST), it was divided into two sections: a high-pressure (HP) stage and a low-pressure (LP) stage. In the design case, the isentropic expansion efficiency for both sections was assumed to be 70% and efficiency calculations were performed using the design efficiency method.

The inlet parameters for each stage were defined accordingly. For the HP section, live steam was introduced at a pressure of 36 bar and a temperature of 500 °C. For the LP section, the inlet pressure of the secondary steam stream was set to 2.7 bar. The deaerator was also supplied with steam at 2.7 bar, drawn from the same line.

In the condenser, the condensate pressure was set to 0.05 bar. A temperature drop of 10 °C was assumed for the cooling water across the condenser unit.

3.8. Model Assumptions and Limitations

The hybrid energy system analyzed in this study was modeled using a set of simplifying assumptions that are necessary to ensure computational tractability and to enable a clear evaluation of system behavior under representative operating conditions. While these assumptions are consistent with common practice in system-level energy modeling, they introduce limitations that should be acknowledged when interpreting the results.

All major subsystems—including the biogas plant, photovoltaic installation, electrolyzer, hydrogen storage, and gas-steam combined-cycle power plant—were modeled under steady-state or quasi-steady-state conditions, assuming ideal operational availability. Unplanned outages, component degradation, and maintenance-related downtime were not explicitly considered. Consequently, the results represent an upper-bound estimate of technical performance under nominal operating conditions.

The electrolysis process was modeled assuming a constant conversion efficiency and linear scaling of hydrogen production with electrical power input. This assumption contributes to the nearly linear relationship observed between electrolyzer power input and hydrogen production. In reality, electrolyzer efficiency may vary with load, temperature, and aging effects; however, these dynamics were neglected due to limited availability of validated, high-resolution performance data for long-term operation.

The gas turbine and steam turbine efficiencies were assumed to remain constant over the analyzed operating range, except for minimum load constraints imposed to ensure stable combustion and steam cycle operation. While real gas turbines typically exhibit

reduced efficiency at partial load, the adopted approach reflects manufacturer-reported nominal performance and enables consistent comparison of different fuel compositions. As a result, efficiency variations at low-load conditions may be underestimated.

The hydrogen storage system was modeled without accounting for leakage, boil-off, or compression losses beyond those implicitly captured in the electrolysis model. Similarly, biomethane storage and buffering effects were not explicitly modeled; instead, continuous availability of upgraded biomethane was assumed based on annual production balances. This approach simplifies operational scheduling but does not capture short-term constraints related to gas storage capacity.

Electricity prices, fuel prices, and policy-driven incentives were assumed to be constant over the analyzed period. Market volatility, dynamic pricing mechanisms, and regulatory uncertainty were not included in the model. Therefore, the study focuses primarily on technical feasibility and energy balance, rather than detailed economic optimization or market-driven dispatch strategies.

The system was assumed to operate with perfect communication and control, neglecting delays or failures in supervisory control systems. Grid interaction was represented in a simplified manner, allowing power exchange without network congestion or curtailment constraints.

Despite these limitations, the adopted modeling framework captures the dominant physical interactions and seasonal dynamics governing integrated biogas–hydrogen–photovoltaic hybrid systems. The results provide valuable insight into system feasibility, operational synergies, and decarbonization potential. Future work should address these limitations by incorporating component degradation models, stochastic failure events, dynamic efficiency curves, economic optimization, and reliability metrics to further enhance the realism and applicability of the proposed hybrid energy system.

4. Results of Calculations and Analyses

4.1. Annual Energy Demand, Renewable Generation, Hydrogen Production and System Operation

The calculations were carried out based on electricity consumption data from the Polish power grid in 2023.

In the initial phase of the analysis, total electricity consumption was examined using data provided by the Polish Power Grid Operator (PSE—Polskie Sieci Elektroenergetyczne). Subsequently, the average hourly electricity consumption for each month was estimated for a representative small municipality with an approximate population of 4500. The results of the calculations in this phase are illustrated in Figure 9.

In the figure, cells colored red indicate peak demand periods, while green cells indicate lower load demands. According to the data, the highest demand occurred during the winter months, particularly in December and January, between 7:00 and 21:00. The lowest demand was observed between April and September, typically during nighttime hours between 00:00 and 06:00.

In the next stage of the calculations, as described in the previous section—"The Description of the Model"—the average hourly electricity generation for each month of 2023 was calculated using data from the EU Photovoltaic Geographical Information System (PVGIS). These calculations were based on a 10 MW peak photovoltaic (PV) installation, using the location coordinates and system parameters specified in that chapter.

As shown in Figure 10, the highest solar yield was recorded in May, particularly between 08:00 and 14:00, highlighted in red. The lowest yield was observed in December.

AVERAGE HOURLY ELECTRICAL ENERGY CONSUMPTION FOR EACH MONTH OF THE YEAR 2023, kWh

Time	Jan	Feb	Mar	Apr	May	Jun	Jul	Aug	Sep	Oct	Nov	Dec
00:00:00	2 022	2 054	2 018	1 838	1 777	1 839	1 804	1 624	1 773	1 916	1 943	2 068
01:00:00	1 962	1 985	1 965	1 771	1 701	1 759	1 724	1 575	1 708	1 856	1 880	1 995
02:00:00	1 928	1 968	1 928	1 732	1 660	1 722	1 685	1 554	1 677	1 815	1 851	1 956
03:00:00	1 909	1 958	1 942	1 737	1 662	1 708	1 667	1 549	1 675	1 830	1 857	1 947
04:00:00	1 944	1 996	1 983	1 781	1 654	1 683	1 664	1 590	1 712	1 873	1 899	1 992
05:00:00	2 055	2 094	2 060	1 851	1 722	1 750	1 708	1 652	1 822	1 986	2 016	2 108
06:00:00	2 370	2 385	2 320	2 131	2 004	2 034	1 969	1 945	2 080	2 299	2 316	2 428
07:00:00	2 597	2 553	2 520	2 351	2 230	2 259	2 195	2 185	2 290	2 499	2 508	2 663
08:00:00	2 703	2 637	2 566	2 440	2 331	2 377	2 318	2 329	2 392	2 593	2 609	2 780
09:00:00	2 754	2 625	2 535	2 429	2 351	2 420	2 339	2 387	2 391	2 562	2 645	2 821
10:00:00	2 767	2 564	2 484	2 360	2 340	2 422	2 353	2 404	2 318	2 458	2 638	2 800
11:00:00	2 816	2 563	2 500	2 369	2 362	2 506	2 381	2 438	2 329	2 403	2 671	2 841
12:00:00	2 826	2 551	2 493	2 368	2 349	2 532	2 372	2 441	2 345	2 378	2 689	2 851
13:00:00	2 825	2 554	2 533	2 370	2 309	2 494	2 335	2 441	2 341	2 381	2 679	2 847
14:00:00	2 761	2 545	2 481	2 333	2 292	2 449	2 279	2 437	2 346	2 373	2 655	2 812
15:00:00	2 736	2 539	2 505	2 333	2 300	2 430	2 310	2 399	2 400	2 406	2 665	2 831
16:00:00	2 783	2 559	2 523	2 338	2 284	2 406	2 309	2 383	2 439	2 451	2 716	2 880
17:00:00	2 803	2 654	2 547	2 313	2 284	2 413	2 283	2 353	2 408	2 510	2 728	2 840
18:00:00	2 761	2 662	2 682	2 349	2 292	2 404	2 310	2 348	2 432	2 624	2 679	2 798
19:00:00	2 729	2 643	2 713	2 408	2 329	2 415	2 346	2 420	2 543	2 651	2 662	2 781
20:00:00	2 643	2 567	2 654	2 457	2 344	2 395	2 353	2 454	2 444	2 571	2 605	2 703
21:00:00	2 486	2 400	2 471	2 293	2 273	2 322	2 256	2 286	2 256	2 392	2 430	2 524
22:00:00	2 324	2 223	2 286	2 104	2 094	2 180	2 119	2 078	2 059	2 203	2 254	2 355
23:00:00	2 167	2 094	2 134	1 955	1 928	1 998	1 959	1 918	1 920	2 047	2 111	2 193

Figure 9. Average hourly electrical energy consumption for each month of the year 2023 in a small municipality with the population of 4500. The background colors represent a heat-map of electricity demand, with green indicating lower consumption, yellow intermediate values, and red higher consumption levels.

AVERAGE HOURLY PV ELECTRICAL ENERGY GENERATION FOR EACH MONTH OF THE YEAR 2023, kWh

Time	Jan	Feb	Mar	Apr	May	Jun	Jul	Aug	Sep	Oct	Nov	Dec
00:00:00	0	0	0	0	0	0	0	0	0	0	0	0
01:00:00	0	0	0	0	0	0	0	0	0	0	0	0
02:00:00	0	0	0	0	0	0	0	0	0	0	0	0
03:00:00	0	0	0	0	12	66	12	0	0	0	0	0
04:00:00	0	0	0	46	253	287	256	100	0	0	0	0
05:00:00	0	0	26	628	1 230	1 250	950	630	440	10	0	0
06:00:00	0	50	814	1 847	2 826	2 698	2 309	2 013	2 043	637	27	0
07:00:00	410	1 047	2 064	3 386	4 199	4 136	3 664	3 270	3 695	1 520	675	41
08:00:00	592	1 469	2 493	4 195	5 457	5 231	4 926	4 257	4 779	2 150	1 115	915
09:00:00	1 143	2 240	3 500	4 604	5 777	5 477	5 499	4 657	5 617	2 223	1 271	1 039
10:00:00	1 028	2 484	3 800	4 500	5 655	5 622	5 471	4 718	5 705	2 491	1 791	630
11:00:00	1 105	2 250	3 559	4 204	5 886	5 270	4 942	4 926	5 827	2 549	1 517	807
12:00:00	757	1 860	3 155	4 142	5 456	5 078	4 525	4 219	5 035	1 840	1 208	596
13:00:00	779	1 941	2 550	3 280	4 928	4 426	3 815	3 477	4 329	1 491	605	307
14:00:00	268	1 655	1 872	2 347	3 653	3 639	2 906	2 564	3 029	892	129	0
15:00:00	0	366	1 047	1 525	2 530	2 676	2 398	1 932	1 545	195	0	0
16:00:00	0	0	107	542	1 012	1 279	1 212	740	246	0	0	0
17:00:00	0	0	0	35	255	391	342	147	0	0	0	0
18:00:00	0	0	0	0	3	91	65	0	0	0	0	0
19:00:00	0	0	0	0	0	0	0	0	0	0	0	0
20:00:00	0	0	0	0	0	0	0	0	0	0	0	0
21:00:00	0	0	0	0	0	0	0	0	0	0	0	0
22:00:00	0	0	0	0	0	0	0	0	0	0	0	0
23:00:00	0	0	0	0	0	0	0	0	0	0	0	0

Figure 10. Average hourly photovoltaic (PV) electrical energy generation for each month of the year 2023. The background colors represent a heat map of PV power output, with green indicating zero or very low generation, yellow moderate generation, and red high generation levels.

By combining residential electricity demand with PV generation, the surplus photovoltaic energy can be used to produce hydrogen through the electrolysis process.

The average hourly hydrogen production for each month is presented in Figure 11.

HYDROGEN PRODUCTION, kg/s

Time	Jan	Feb	Mar	Apr	May	Jun	Jul	Aug	Sep	Oct	Nov	Dec
00:00:00	0	0	0	0	0	0	0	0	0	0	0	0
01:00:00	0	0	0	0	0	0	0	0	0	0	0	0
02:00:00	0	0	0	0	0	0	0	0	0	0	0	0
03:00:00	0	0	0	0	0	0	0	0	0	0	0	0
04:00:00	0	0	0	0	0	0	0	0	0	0	0	0
05:00:00	0	0	0	0	0	0	0	0	0	0	0	0
06:00:00	0	0	0	0	0.005	0.004	0.002	0	0	0	0	0
07:00:00	0	0	0	0.007	0.013	0.012	0.009	0.007	0.009	0	0	0
08:00:00	0	0	0	0.011	0.020	0.018	0.017	0.012	0.015	0	0	0
09:00:00	0	0	0.006	0.014	0.022	0.019	0.020	0.014	0.020	0	0	0
10:00:00	0	0	0.008	0.014	0.021	0.020	0.020	0.014	0.021	0	0	0
11:00:00	0	0	0.007	0.012	0.022	0.018	0.016	0.016	0.022	0	0	0
12:00:00	0	0	0.004	0.011	0.020	0.016	0.014	0.012	0.017	0	0	0
13:00:00	0	0	0	0.006	0.017	0.012	0.009	0.007	0.013	0	0	0
14:00:00	0	0	0	0	0.009	0.008	0.004	0	0.004	0	0	0
15:00:00	0	0	0	0	0	0	0	0	0	0	0	0
16:00:00	0	0	0	0	0	0	0	0	0	0	0	0
17:00:00	0	0	0	0	0	0	0	0	0	0	0	0
18:00:00	0	0	0	0	0	0	0	0	0	0	0	0
19:00:00	0	0	0	0	0	0	0	0	0	0	0	0
20:00:00	0	0	0	0	0	0	0	0	0	0	0	0
21:00:00	0	0	0	0	0	0	0	0	0	0	0	0
22:00:00	0	0	0	0	0	0	0	0	0	0	0	0
23:00:00	0	0	0	0	0	0	0	0	0	0	0	0
Daily, kg	0	0	92	267	531	459	401	295	440	0	0	0

Figure 11. Average hourly hydrogen production for each month. The background colors represent a heat map of hydrogen production rate, with green indicating zero or very low production, yellow moderate production, and red high production levels.

As shown in the figure, hydrogen production is feasible between March and September, with the highest daily production reaching approximately 531 kg in May. Additionally, the figure indicates that the average annual hydrogen production amounts to approximately 75.87 t.

Since the maximum daily production was recorded in May, the hydrogen energy storage system is considered to have a daily capacity of 550 kg, including a 19 kg buffer.

The stored hydrogen is then distributed equally across the hours when there is no solar energy production, blending with biomethane for combustion in the gas turbine's combustion chamber.

This situation is analyzed using the example of the energy balance in May. The average hourly energy consumption and production balance data are illustrated in Table 5. According to the data provided, between 06:00 and 16:00, photovoltaic (PV) generation meets the grid consumption and produces surplus electricity, which is used for hydrogen production, as shown in Figure 12.

Table 5. Average hourly energy consumption-production balance data in May. Light orange cells highlight hours in which the gas-steam unit operates below its nominal load.

MAY											
Time	Consumption	GT Power	ST Power	Gas-Steam Power	GT Effi-ciency	Gas-Steam Efficiecny	Fuel Mix Mass Flow	Exhaust Mass Flow	Live Steam Mass Flow	H_2 Mass Prop	CH_4 Mass Prop
	kWh	kWh	kWh	kWh	%	%	kg/s	kg/s	kg/s	%	%
00:00:00	1700	1115	585	1700	29.19	44.55	0.0631	4.7430	0.6400	15.0	85.0
01:00:00	1700	1115	585	1700	29.19	44.55	0.0631	4.7430	0.6400	15.0	85.0

Table 5. *Cont.*

MAY											
Time	Consumption	GT Power	ST Power	Gas-Steam Power	GT Effi-ciency	Gas-Steam Efficiecny	Fuel Mix Mass Flow	Exhaust Mass Flow	Live Steam Mass Flow	H_2 Mass Prop	CH_4 Mass Prop
	kWh	kWh	kWh	kWh	%	%	kg/s	kg/s	kg/s	%	%
02:00:00	1700	1115	585	1700	29.19	44.55	0.0631	4.7430	0.6400	15.0	85.0
03:00:00	1700	1115	585	1700	29.19	44.55	0.0631	4.7430	0.6400	15.0	85.0
04:00:00	1400	891	466	1357	29.24	44.52	0.0487	3.7790	0.5112	18.0	82.0
05:00:00	500	891	466	1357	29.24	44.52	0.0487	3.7790	0.5112	18.0	82.0
06:00:00	0	0	0	0	0.00	0.00	0.0000	0.0000	0.0000	0.0	0.0
07:00:00	0	0	0	0	0.00	0.00	0.0000	0.0000	0.0000	0.0	0.0
08:00:00	0	0	0	0	0.00	0.00	0.0000	0.0000	0.0000	0.0	0.0
09:00:00	0	0	0	0	0.00	0.00	0.0000	0.0000	0.0000	0.0	0.0
10:00:00	0	0	0	0	0.00	0.00	0.0000	0.0000	0.0000	0.0	0.0
11:00:00	0	0	0	0	0.00	0.00	0.0000	0.0000	0.0000	0.0	0.0
12:00:00	0	0	0	0	0.00	0.00	0.0000	0.0000	0.0000	0.0	0.0
13:00:00	0	0	0	0	0.00	0.00	0.0000	0.0000	0.0000	0.0	0.0
14:00:00	0	0	0	0	0.00	0.00	0.0000	0.0000	0.0000	0.0	0.0
15:00:00	0	0	0	0	0.00	0.00	0.0000	0.0000	0.0000	0.0	0.0
16:00:00	1300	891	466	1357	29.24	44.52	0.0487	3.7790	0.5112	18.0	82.0
17:00:00	2000	1306	694	2000	29.15	44.66	0.0758	5.5710	0.7550	13.0	87.0
18:00:00	2300	1505	795	2300	29.09	44.44	0.0907	6.4460	0.8610	10.0	90.0
19:00:00	2300	1505	795	2300	29.09	44.44	0.0907	6.4460	0.8610	10.0	90.0
20:00:00	2300	1505	795	2300	29.09	44.44	0.0907	6.4460	0.8610	10.0	90.0
21:00:00	2300	1505	795	2300	29.09	44.44	0.0907	6.4460	0.8610	10.0	90.0
22:00:00	2000	1306	694	2000	29.15	44.66	0.7575	5.5710	0.7550	13.0	87.0
23:00:00	2000	1306	694	2000	29.15	44.66	0.7575	5.5710	0.7550	13.0	87.0

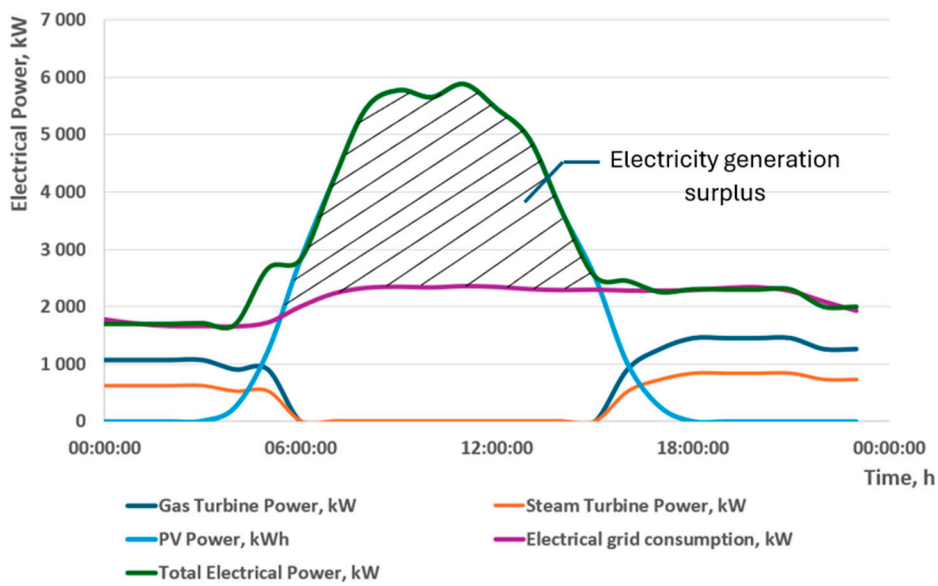

Figure 12. Average hourly energy consumption-production balance in May.

During the remaining hours—from 16:00 to 06:00—the previously generated hydrogen is distributed evenly. The hydrogen proportion in the biomethane-hydrogen mix varies depending on the fuel mass flow rate, which is determined by the power load for electricity consumption and production.

As shown, between 00:00 and 04:00, the hydrogen mass proportion in the fuel mix is approximately 15%. Between 04:00 and 06:00, it increases to 18%, while between 18:00 and 22:00, the hydrogen share in the mix is about 10%.

During periods of low electrical grid consumption, the gas-steam system operates under certain technical limitations related to the minimum load requirements of the gas and steam turbines.

Specifically, for the 100% biomethane-powered case, the minimum operational load is 875 kW for the gas turbine and 467 kW for the steam turbine.

For cases powered by the hydrogen/biomethane fuel mix, these minimum load values vary depending on the fuel composition:

Gas turbine: from 887 kW to 937 kW

Steam turbine: from 466 kW to 493 kW

These variations reflect the influence of the hydrogen-to-biomethane ratio in the fuel mix on turbine performance.

As a result, even during hours with relatively low energy demand—such as from 04:00 to 05:00, from 05:00 to 06:00, and between 16:00 and 17:00, when the electrical consumption is 1400 kWh, 500 kWh, and 1300 kWh respectively—the gas-steam system still generates a constant electrical power output of 1438 kWh. The excess energy produced during these times is sold to the grid.

In Figure 12, the power outputs of the gas turbine, steam turbine and PV system are illustrated alongside the electrical grid consumption. The figure clearly shows both the excess energy produced by the gas-steam system and the surplus electricity generated by the PV installation.

In contrast, the situation is different during months without surplus PV generation.

This can be illustrated using the example of January. The average hourly energy consumption-production balance is shown in Figure 13. As there is no excess electricity generation during this month, hydrogen production does not occur. Consequently, the grid demand is met entirely by the gas-steam system, using 100% biomethane in the gas turbine's combustion chamber and a portion of the demand is also met directly by PV generation.

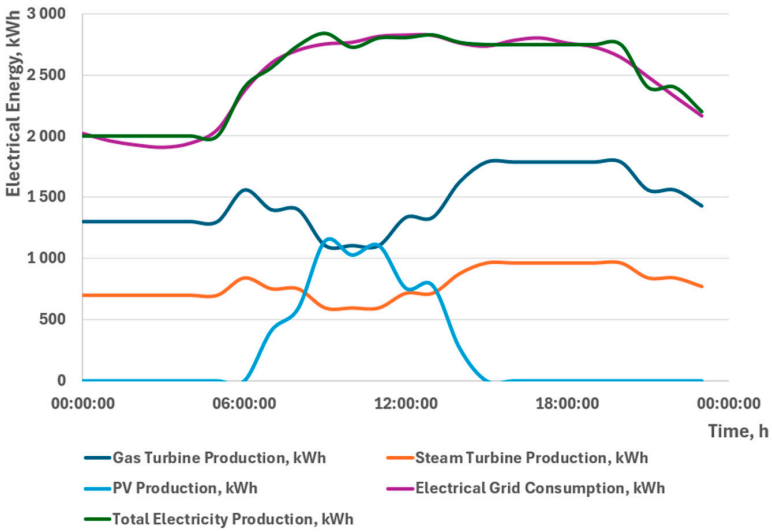

Figure 13. Average hourly energy consumption-production balance in January.

The average hourly energy consumption-production balance data were calculated for each month of the year and are provided separately for each month in the Appendix A of this work.

4.2. CO_2 Emissions and Emissions Reduction Assessment

To quantify the environmental benefits of the proposed hybrid energy system, an operational CO_2 emissions assessment was conducted by comparing the analyzed system with a conventional grid-based electricity supply scenario. The assessment focuses on direct operational emissions associated with electricity generation and excludes upstream construction-related emissions, consistent with the scope and system boundaries of this study.

4.2.1. Reference Case: Grid-Based Electricity Supply

The reference case assumes that the annual electricity demand of the settlement is fully supplied by the national electricity grid. Based on the calculated average electricity consumption of approximately 2.8–3.2 MWh per capita per year and a population of 4500 inhabitants, the total annual electricity demand E_{ann} is estimated as:

$$E_{ann} = N_{pop} \times e_{cap} \tag{3}$$

$$E_{ann} = 4500 \times 3.0 \approx 13,500\ MWh/year \tag{4}$$

For the Polish electricity system, an average grid emission factor EF_{grid} of 0.70 tCO_2/MWh was adopted, reflecting the coal-dominated generation mix in 2023. The annual operational CO_2 emissions of the reference case $CO_{2,ref}$ were calculated as:

$$CO_{2,ref} = E_{ann} \times EF_{grid} \tag{5}$$

$$CO_{2,ref} = 13,500 \times 0.70 \approx 9450\ tCO_2/year \tag{6}$$

4.2.2. Hybrid System Operational Emissions

In the proposed hybrid energy system, electricity is generated primarily from photovoltaic power, biomethane-fueled gas-steam combined-cycle operation, and hydrogen-assisted combustion. Photovoltaic electricity generation and hydrogen produced via renewable-powered electrolysis are considered zero-emission at the point of use. Biomethane combustion is treated as carbon-neutral under operational accounting, as the released CO_2 originates from biogenic carbon previously absorbed during biomass growth.

Accordingly, the annual operational CO_2 emissions of the hybrid system $CO_{2,hyb}$ are limited to auxiliary electricity consumption and residual grid interactions and can be expressed as:

$$CO_{2,hyb} \approx CO_{2,aux} + CO_{2,grid,res} \tag{7}$$

Based on the annual energy balance results, these emissions were estimated to be approximately:

$$CO_{2,hyb} \approx 650\ tCO_2/year \tag{8}$$

4.2.3. CO_2 Emissions Reduction

The absolute annual CO_2 emissions reduction ΔCO_2 achieved by the proposed hybrid system is calculated as:

$$\Delta CO_2 = CO_{2,ref} - CO_{2hyb} \tag{9}$$

$$\Delta CO_2 = 9450 - 650 \approx 8800\ tCO_2/year \tag{10}$$

The relative CO_2 emissions reduction R_{CO2} is given by:

$$R_{CO2} = \frac{\Delta CO_2}{CO_{2,ref}} \times 100\% \tag{11}$$

$$R_{CO2} \approx \frac{8800}{9450} \times 100\% \approx 93\% \quad (12)$$

4.2.4. Discussion

These results demonstrate the strong decarbonization potential of integrated biogas–hydrogen–photovoltaic hybrid energy systems for small municipalities, particularly in regions characterized by carbon-intensive electricity grids. The combination of renewable electricity generation, long-duration hydrogen storage, and dispatchable biomethane-supported power production enables a near-complete elimination of operational CO_2 emissions while maintaining reliable, year-round electricity supply.

5. Conclusions

This study investigated the technical feasibility and decarbonization potential of a fully integrated hybrid energy system combining biogas upgrading to biomethane, photovoltaic electricity generation, hydrogen production via alkaline electrolysis, hydrogen storage, and a gas-steam combined-cycle power plant. The system was designed to supply uninterrupted electricity to a small municipality of approximately 4500 inhabitants under predominantly self-sufficient operating conditions.

Using full-year, high-resolution electricity demand data and satellite-based meteorological inputs for 2023, detailed process-based simulations were conducted in Aspen Plus and Aspen HYSYS. The results demonstrate that a hybrid configuration consisting of a 10 MWp photovoltaic installation, a 2.9 MW gas-steam combined-cycle unit, and 550 kg of hydrogen storage can reliably meet annual electricity demand. During spring and summer months, surplus photovoltaic electricity enables hydrogen production, while winter operation is fully supported by dispatchable biomethane-fueled power generation. Hydrogen co-firing enhances operational flexibility and supports load-following operation without compromising system stability.

The annual energy balance indicates that hydrogen production is feasible primarily between March and September, with an average annual hydrogen output of approximately 75.9 t and a maximum daily production of about 531 kg in May. The imposed hydrogen storage capacity ensures effective redistribution of renewable energy during non-solar hours, reducing reliance on grid electricity and enabling high renewable energy utilization throughout the year

From an environmental perspective, the proposed hybrid system achieves a substantial reduction in operational CO_2 emissions. Compared to a conventional grid-based electricity supply, characterized by a carbon-intensive generation mix, the hybrid system reduces annual operational CO_2 emissions by approximately 8800 tCO_2, corresponding to a reduction of about 93%. This result highlights the strong decarbonization potential of integrated biogas–hydrogen–photovoltaic systems for small communities, particularly in regions with limited grid decarbonization.

Several limitations of the present study should be acknowledged. The analysis assumes idealized component availability and steady-state operation, neglecting equipment degradation, unplanned outages, and dynamic efficiency variations at part-load conditions. Economic optimization, market price volatility, and reliability metrics were not explicitly considered, and the assessment focused primarily on operational rather than full life-cycle emissions.

Future research should extend the proposed framework by incorporating techno-economic optimization, stochastic modeling of component failures, dynamic efficiency curves, and detailed reliability indicators. Further investigation into alternative energy storage pathways, such as biogas-based energy storage or sector-coupled applications, as well as policy and regulatory impacts, would enhance the practical relevance of such systems.

Nevertheless, the findings of this study demonstrate that fully integrated hybrid energy systems can provide a scalable, low-carbon, and dispatchable solution for decentralized electricity supply in rural and semi-urban communities.

Author Contributions: Conceptualization, A.H. and Ł.S.; Methodology, A.H., K.B. and Ł.S.; Software, A.H. and Ł.S.; Validation, A.H.; Formal analysis, A.H.; Investigation, A.H.; Resources, A.H.; Data curation, A.H.; Writing—original draft, A.H.; Writing—review & editing, A.H.; Visualization, A.H., K.B. and Ł.S.; Supervision, K.B. and Ł.S.; Project administration, K.B. and Ł.S.; Funding acquisition, K.B. All authors have read and agreed to the published version of the manuscript.

Funding: This research was funded by Warsaw University of Technology within the Excellence Initiative: Research University (IDUB) program.

Data Availability Statement: The data presented in this study are available on request from the corresponding author.

Conflicts of Interest: The authors declare no conflict of interest.

Appendix A.

Appendix A.1. Average Hourly Energy Consumption-Production Balance in January

JANUARY									
Time	Consumption	GT Power Output	ST Power Output	Gas-Steam Power Output	GT Efficiency	Gas-Steam Efficiency	Biomethane Mass Flow	Exhaust Mass Flow	Live Steam Mass Flow
	kWh	kWh	kWh	kWh	%	%	kg/s	kg/s	kg/s
00:00:00	2000	1301	699	2000	28.85	44.38	0.0901	5.6600	0.7610
01:00:00	2000	1301	699	2000	28.85	44.38	0.0901	5.6600	0.7610
02:00:00	2000	1301	699	2000	28.85	44.38	0.0901	5.6600	0.7610
03:00:00	2000	1301	699	2000	28.85	44.38	0.0901	5.6600	0.7610
04:00:00	2000	1301	699	2000	28.85	44.38	0.0901	5.6600	0.7610
05:00:00	2000	1301	699	2000	28.85	44.38	0.0901	5.6600	0.7610
06:00:00	2400	1558	842	2400	28.85	44.45	0.1079	6.7830	0.9130
07:00:00	2150	1398	752	2150	28.85	44.37	0.0969	6.0870	0.8160
08:00:00	2150	1398	752	2150	28.85	44.37	0.0969	6.0870	0.8160
09:00:00	1700	1106	594	1700	28.85	44.32	0.0766	4.8170	0.6470
10:00:00	1700	1106	594	1700	28.85	44.32	0.0766	4.8170	0.6470
11:00:00	1700	1106	594	1700	28.85	44.32	0.0766	4.8170	0.6470
12:00:00	2050	1335	715	2050	28.85	44.31	0.0925	5.8120	0.7770
13:00:00	2050	1335	715	2050	28.85	44.31	0.0925	5.8120	0.7770
14:00:00	2500	1623	877	2500	28.85	44.46	0.1124	7.0620	0.9500
15:00:00	2750	1785	965	2750	28.85	44.46	0.1236	7.7690	1.0440
16:00:00	2750	1785	965	2750	28.85	44.46	0.1236	7.7690	1.0440
17:00:00	2750	1785	965	2750	28.85	44.46	0.1236	7.7690	1.0440
18:00:00	2750	1785	965	2750	28.85	44.46	0.1236	7.7690	1.0440
19:00:00	2750	1785	965	2750	28.85	44.46	0.1236	7.7690	1.0440
20:00:00	2750	1785	965	2750	28.85	44.46	0.1236	7.7690	1.0440
21:00:00	2400	1558	842	2400	28.85	44.45	0.1079	6.7830	0.9130
22:00:00	2400	1558	842	2400	28.85	44.45	0.1079	6.7830	0.9130
23:00:00	2200	1429	771	2200	28.85	44.43	0.0990	6.2190	0.8370

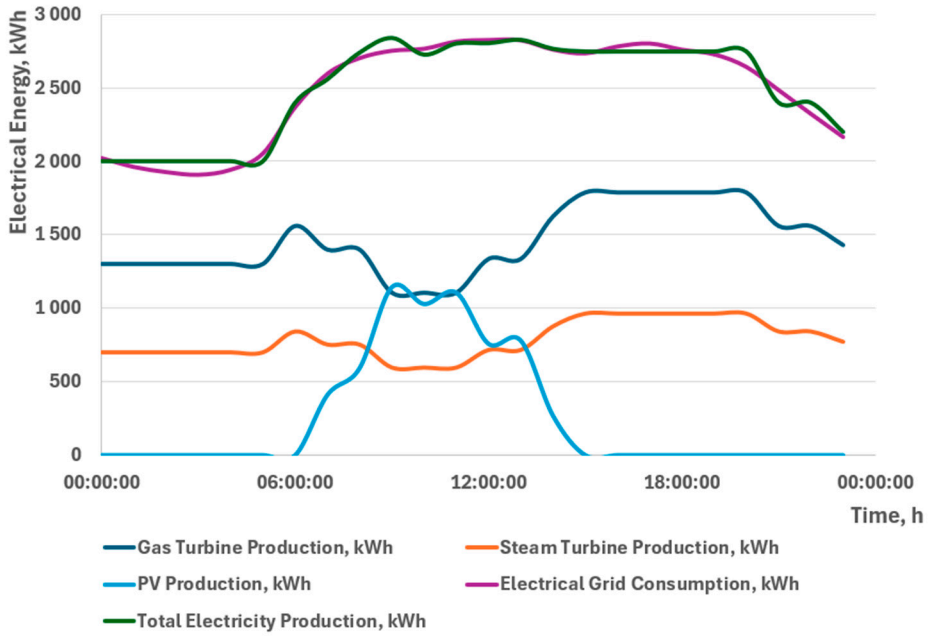

Appendix A.2. Average Hourly Energy Consumption-Production Balance in February

FEBRUARY									
Time	Consumption	GT Power Output	ST Power Output	Gas-Steam Power Output	GT Efficiency	Gas-Steam Efficiency	Biomethane Mass Flow	Exhaust Mass Flow	Live Steam Mass Flow
	kWh	kWh	kWh	kWh	%	%	kg/s	kg/s	kg/s
00:00:00	2000	1301	699	2000	28.85	44.38	0.0901	5.6600	0.7610
01:00:00	2000	1301	699	2000	28.85	44.38	0.0901	5.6600	0.7610
02:00:00	2000	1301	699	2000	28.85	44.38	0.0901	5.6600	0.7610
03:00:00	2000	1301	699	2000	28.85	44.38	0.0901	5.6600	0.7610
04:00:00	2000	1301	699	2000	28.85	44.38	0.0901	5.6600	0.7610
05:00:00	2000	1301	699	2000	28.85	44.38	0.0901	5.6600	0.7610
06:00:00	2350	1527	823	2350	28.85	44.42	0.1057	6.6460	0.8930
07:00:00	1500	980	520	1500	28.85	44.17	0.0679	4.2680	0.5700
08:00:00	1200	875	467	1342	28.85	44.23	0.0606	3.8110	0.5120
09:00:00	250	875	467	1342	28.85	44.23	0.0606	3.8110	0.5120
10:00:00	250	875	467	1342	28.85	44.23	0.0606	3.8110	0.5120
11:00:00	250	875	467	1342	28.85	44.23	0.0606	3.8110	0.5120
12:00:00	650	875	467	1342	28.85	44.23	0.0606	3.8110	0.5120
13:00:00	650	875	467	1342	28.85	44.23	0.0606	3.8110	0.5120
14:00:00	1000	875	467	1342	28.85	44.23	0.0606	3.8110	0.5120
15:00:00	2200	1429	771	2200	28.85	44.43	0.0990	6.2190	0.8370
16:00:00	2600	1685	915	2600	28.85	44.52	0.1167	7.3370	0.9900
17:00:00	2600	1685	915	2600	28.85	44.52	0.1167	7.3370	0.9900
18:00:00	2600	1685	915	2600	28.85	44.52	0.1167	7.3370	0.9900
19:00:00	2600	1685	915	2600	28.85	44.52	0.1167	7.3370	0.9900
20:00:00	2600	1685	915	2600	28.85	44.52	0.1167	7.3370	0.9900
21:00:00	2600	1685	915	2600	28.85	44.52	0.1167	7.3370	0.9900
22:00:00	2200	1429	771	2200	28.85	44.43	0.0990	6.2190	0.8370
23:00:00	2100	1365	735	2100	28.85	44.41	0.0946	5.9450	0.8000

Light orange cells highlight hours in which the gas-steam unit operates below its nominal load.

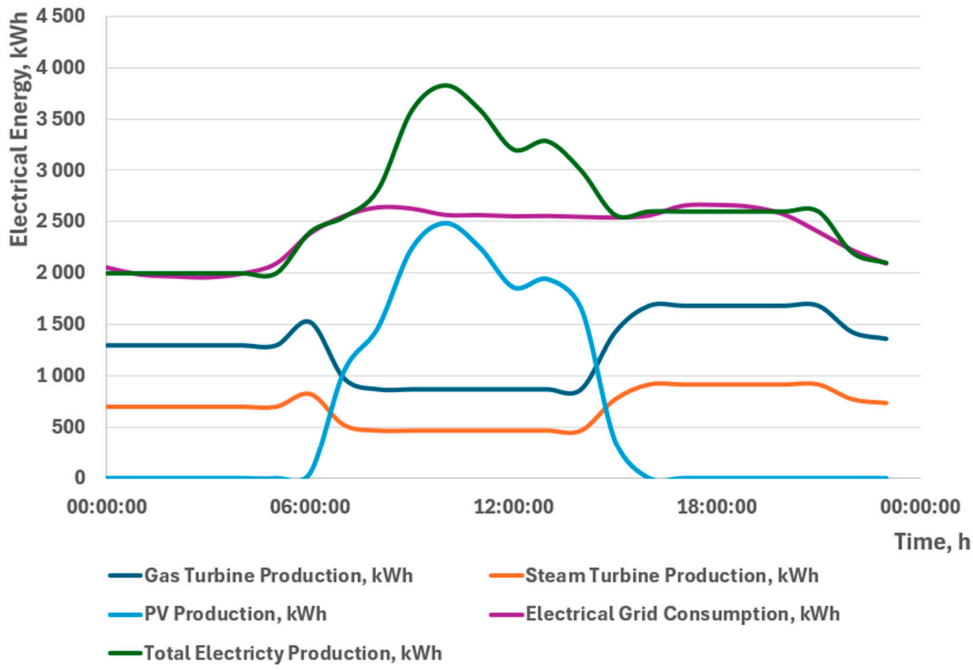

Appendix A.3. Average Hourly Energy Consumption-Production Balance in March

MARCH											
Time	Consumption	GT Power Output	ST Power Output	Gas-Steam Power Output	GT Efficiency	Gas-Steam Efficiency	Fuel Mix Mass Flow	Exhaust Mass Flow	Live Steam Mass Flow	H_2 Mass Prop	CH_4 Mass Prop
	kWh	kWh	kWh	kWh	%	%	kg/s	kg/s	kg/s	%	%
00:00:00	2000	1300	700	2000	28.89	44.46	0.0881	5.6430	0.7610	1.5	98.5
01:00:00	2000	1300	700	2000	28.89	44.46	0.0881	5.6430	0.7610	1.5	98.5
02:00:00	2000	1300	700	2000	28.89	44.46	0.0881	5.6430	0.7610	1.5	98.5
03:00:00	2000	1300	700	2000	28.89	44.46	0.0881	5.6430	0.7610	1.5	98.5
04:00:00	2000	1300	700	2000	28.89	44.46	0.0881	5.6430	0.7610	1.5	98.5
05:00:00	2000	1300	700	2000	28.89	44.46	0.0881	5.6430	0.7610	1.5	98.5
06:00:00	1500	979	521	1500	28.91	44.29	0.0066	4.2460	0.5700	2.1	98.0
07:00:00	500	937	493	1430	28.91	44.12	0.0629	4.0630	0.5400	2.1	97.9
08:00:00	100	937	493	1430	28.91	44.12	0.0629	4.0630	0.5400	2.1	97.9
09:00:00	0	0	0	0	0.00	0.00	0.0000	0.0000	0.0000	0.0	0.0
10:00:00	0	0	0	0	0.00	0.00	0.0000	0.0000	0.0000	0.0	0.0
11:00:00	0	0	0	0	0.00	0.00	0.0000	0.0000	0.0000	0.0	0.0
12:00:00	0	0	0	0	0.00	0.00	0.0000	0.0000	0.0000	0.0	0.0
13:00:00	0	0	0	0	0.00	0.00	0.0000	0.0000	0.0000	0.0	0.0
14:00:00	600	937	493	1430	28.91	44.12	0.0629	4.0630	0.5400	2.1	97.9
15:00:00	1500	979	521	1500	28.91	44.29	0.0066	4.2460	0.5700	2.1	98.0
16:00:00	2600	1689	911	2600	28.89	44.47	0.1149	7.2200	0.9860	1.2	98.8
17:00:00	2600	1689	911	2600	28.89	44.47	0.1149	7.2200	0.9860	1.2	98.8
18:00:00	2600	1689	911	2600	28.89	44.47	0.1149	7.2200	0.9860	1.2	98.8
19:00:00	2600	1689	911	2600	28.89	44.47	0.1149	7.2200	0.9860	1.2	98.8
20:00:00	2600	1689	911	2600	28.89	44.47	0.1149	7.2200	0.9860	1.2	98.8
21:00:00	2600	1689	911	2600	28.89	44.47	0.1149	7.2200	0.9860	1.2	98.8
22:00:00	2300	1498	802	2300	28.89	44.37	0.1017	6.4000	0.8700	1.3	98.7
23:00:00	2150	1404	746	2150	28.89	44.25	0.0954	6.0950	0.8100	1.4	98.6

Light orange cells highlight hours in which the gas-steam unit operates below its nominal load.

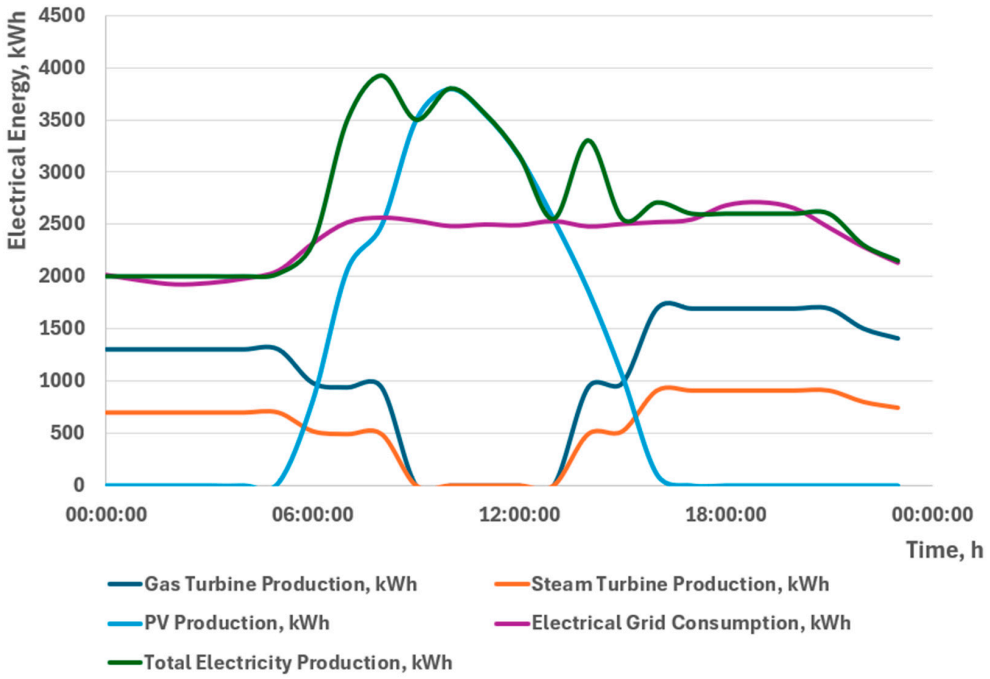

Appendix A.4. Average Hourly Energy Consumption-Production Balance in April

APRIL											
Time	Consumption	GT Power Output	ST Power Output	Gas-Steam Power Output	GT Efficiency	Gas-Steam Efficiency	Fuel Mix Mass Flow	Exhaust Mass Flow	Live Steam Mass Flow	H_2 Mass Prop	CH_4 Mass Prop
	kWh	kWh	kWh	kWh	%	%	kg/s	kg/s	kg/s	%	%
00:00:00	1850	1207	643	1850	29.01	44.46	0.0766	5.2020	0.7000	6.2	93.9
01:00:00	1750	1145	605	1750	29.02	44.37	0.0721	4.9270	0.6600	6.6	93.4
02:00:00	1750	1145	605	1750	29.02	44.37	0.0721	4.9270	0.6600	6.6	93.4
03:00:00	1750	1145	605	1750	29.02	44.37	0.0721	4.9270	0.6600	6.6	93.4
04:00:00	1750	1145	605	1750	29.02	44.37	0.0721	4.9270	0.6600	6.6	93.4
05:00:00	1250	893	467	1360	29.06	44.23	0.0551	3.7800	0.5120	8.2	91.8
06:00:00	300	893	467	1360	29.06	44.23	0.0551	3.7800	0.5120	8.2	91.8
07:00:00	0	0	0	0	0.00	0.00	0.0000	0.0000	0.0000	0.0	0.0
08:00:00	0	0	0	0	0.00	0.00	0.0000	0.0000	0.0000	0.0	0.0
09:00:00	0	0	0	0	0.00	0.00	0.0000	0.0000	0.0000	0.0	0.0
10:00:00	0	0	0	0	0.00	0.00	0.0000	0.0000	0.0000	0.0	0.0
11:00:00	0	0	0	0	0.00	0.00	0.0000	0.0000	0.0000	0.0	0.0
12:00:00	0	0	0	0	0.00	0.00	0.0000	0.0000	0.0000	0.0	0.0
13:00:00	0	0	0	0	0.00	0.00	0.0000	0.0000	0.0000	0.0	0.0
14:00:00	0	0	0	0	0.00	0.00	0.0000	0.0000	0.0000	0.0	0.0
15:00:00	800	893	467	1360	29.06	44.23	0.0551	3.7800	0.5120	8.2	91.8
16:00:00	1800	1178	622	1800	29.01	44.31	0.0745	5.0740	0.6770	6.4	93.6
17:00:00	2400	1561	839	2400	28.97	44.55	0.1010	6.7410	0.9090	4.7	95.3
18:00:00	2400	1561	839	2400	28.97	44.55	0.1010	6.7410	0.9090	4.7	95.3
19:00:00	2400	1561	839	2400	28.97	44.55	0.1010	6.7410	0.9090	4.7	95.3
20:00:00	2400	1561	839	2400	28.97	44.55	0.1010	6.7410	0.9090	4.7	95.3
21:00:00	2400	1561	839	2400	28.97	44.55	0.1010	6.7410	0.9090	4.7	95.3
22:00:00	2050	1337	713	2050	28.99	44.46	0.0855	5.7660	0.7750	5.5	94.5
23:00:00	2050	1337	713	2050	28.99	44.46	0.0855	5.7660	0.7750	5.5	94.5

Light orange cells highlight hours in which the gas-steam unit operates below its nominal load.

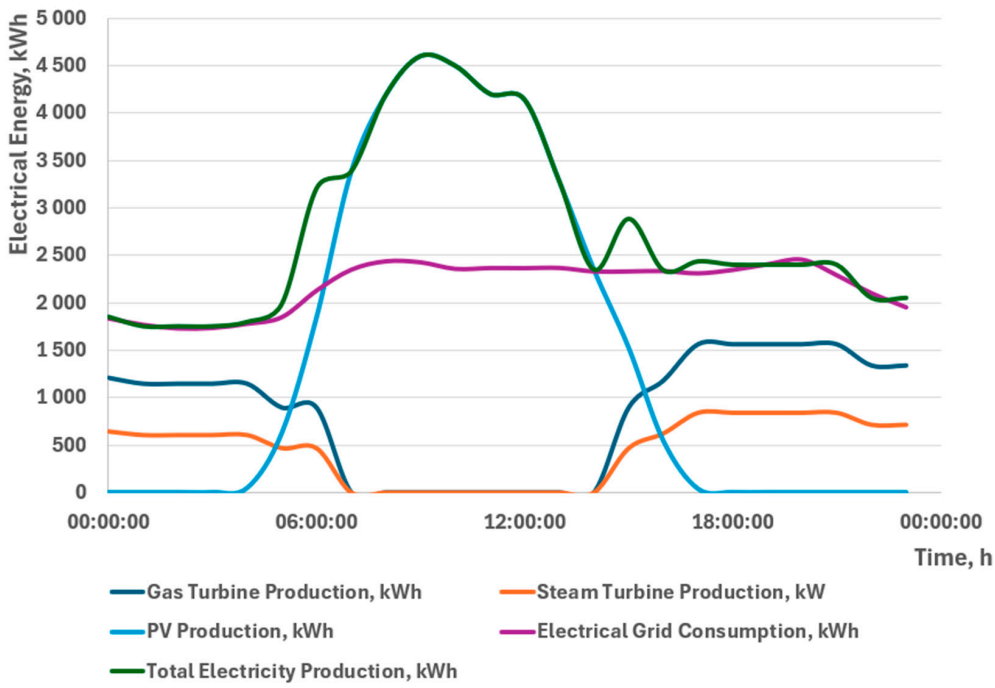

Appendix A.5. Average Hourly Energy Consumption-Production Balance in May

MAY											
Time	Consumption	GT Power Output	ST Power Output	Gas-Steam Power Output	GT Efficiency	Gas-Steam Efficiency	Fuel Mix Mass Flow	Exhaust Mass Flow	Live Steam Mass Flow	H_2 Mass Prop	CH_4 Mass Prop
	kWh	kWh	kWh	kWh	%	%	kg/s	kg/s	kg/s	%	%
00:00:00	1700	1115	585	1700	29.19	44.55	0.0631	4.7430	0.6400	15.0	85.0
01:00:00	1700	1115	585	1700	29.19	44.55	0.0631	4.7430	0.6400	15.0	85.0
02:00:00	1700	1115	585	1700	29.19	44.55	0.0631	4.7430	0.6400	15.0	85.0
03:00:00	1700	1115	585	1700	29.19	44.55	0.0631	4.7430	0.6400	15.0	85.0
04:00:00	1400	891	466	1357	29.24	44.52	0.0487	3.7790	0.5112	18.0	82.0
05:00:00	500	891	466	1357	29.24	44.52	0.0487	3.7790	0.5112	18.0	82.0
06:00:00	0	0	0	0	0.00	0.00	0.0000	0.0000	0.0000	0.0	0.0
07:00:00	0	0	0	0	0.00	0.00	0.0000	0.0000	0.0000	0.0	0.0
08:00:00	0	0	0	0	0.00	0.00	0.0000	0.0000	0.0000	0.0	0.0
09:00:00	0	0	0	0	0.00	0.00	0.0000	0.0000	0.0000	0.0	0.0
10:00:00	0	0	0	0	0.00	0.00	0.0000	0.0000	0.0000	0.0	0.0
11:00:00	0	0	0	0	0.00	0.00	0.0000	0.0000	0.0000	0.0	0.0
12:00:00	0	0	0	0	0.00	0.00	0.0000	0.0000	0.0000	0.0	0.0
13:00:00	0	0	0	0	0.00	0.00	0.0000	0.0000	0.0000	0.0	0.0
14:00:00	0	0	0	0	0.00	0.00	0.0000	0.0000	0.0000	0.0	0.0
15:00:00	0	0	0	0	0.00	0.00	0.0000	0.0000	0.0000	0.0	0.0
16:00:00	1300	891	466	1357	29.24	44.52	0.0487	3.7790	0.5112	18.0	82.0
17:00:00	2000	1306	694	2000	29.15	44.66	0.0758	5.5710	0.7550	13.0	87.0
18:00:00	2300	1505	795	2300	29.09	44.44	0.0907	6.4460	0.8610	10.0	90.0
19:00:00	2300	1505	795	2300	29.09	44.44	0.0907	6.4460	0.8610	10.0	90.0
20:00:00	2300	1505	795	2300	29.09	44.44	0.0907	6.4460	0.8610	10.0	90.0
21:00:00	2300	1505	795	2300	29.09	44.44	0.0907	6.4460	0.8610	10.0	90.0
22:00:00	2000	1306	694	2000	29.15	44.66	0.7575	5.5710	0.7550	13.0	87.0
23:00:00	2000	1306	694	2000	29.15	44.66	0.7575	5.5710	0.7550	13.0	87.0

Light orange cells highlight hours in which the gas-steam unit operates below its nominal load.

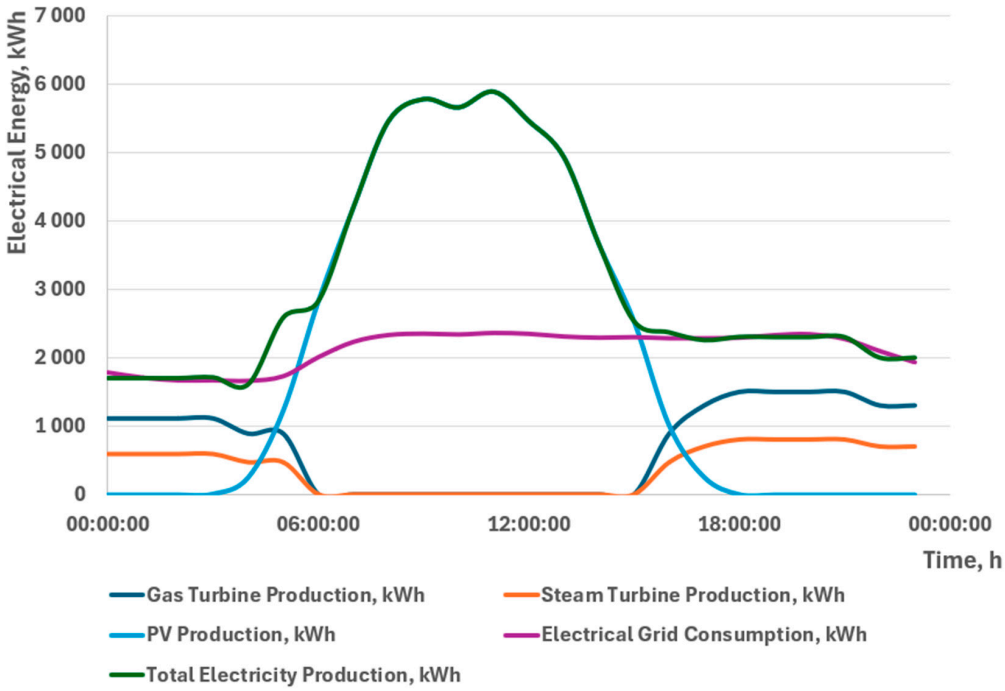

Appendix A.6. Average Hourly Energy Consumption-Production Balance in June

JUNE											
Time	Consumption	GT Power Output	ST Power Output	Gas-Steam Power Output	GT Efficiency	Gas-Steam Efficiency	Fuel mix Mass Flow	Exhaust Mass Flow	Live Steam Mass Flow	H_2 Mass Prop	CH_4 Mass Prop
	kWh	kWh	kWh	kWh	%	%	kg/s	kg/s	kg/s	%	%
00:00:00	1750	1143	607	1750	29.15	44.62	0.0663	4.8760	0.6610	13.0	87.0
01:00:00	1750	1143	607	1750	29.15	44.62	0.0663	4.8760	0.6610	13.0	87.0
02:00:00	1750	1143	607	1750	29.15	44.62	0.0663	4.8760	0.6610	13.0	87.0
03:00:00	1750	1143	607	1750	29.15	44.62	0.0663	4.8760	0.6610	13.0	87.0
04:00:00	1400	889	466	1355	29.23	44.57	0.0491	3.7710	0.5120	17.0	83.0
05:00:00	500	889	466	1355	29.23	44.57	0.0491	3.7710	0.5120	17.0	83.0
06:00:00	0	0	0	0	0.00	0.00	0.0000	0.0000	0.0000	0.0	0.0
07:00:00	0	0	0	0	0.00	0.00	0.0000	0.0000	0.0000	0.0	0.0
08:00:00	0	0	0	0	0.00	0.00	0.0000	0.0000	0.0000	0.0	0.0
09:00:00	0	0	0	0	0.00	0.00	0.0000	0.0000	0.0000	0.0	0.0
10:00:00	0	0	0	0	0.00	0.00	0.0000	0.0000	0.0000	0.0	0.0
11:00:00	0	0	0	0	0.00	0.00	0.0000	0.0000	0.0000	0.0	0.0
12:00:00	0	0	0	0	0.00	0.00	0.0000	0.0000	0.0000	0.0	0.0
13:00:00	0	0	0	0	0.00	0.00	0.0000	0.0000	0.0000	0.0	0.0
14:00:00	0	0	0	0	0.00	0.00	0.0000	0.0000	0.0000	0.0	0.0
15:00:00	0	0	0	0	0.00	0.00	0.0000	0.0000	0.0000	0.0	0.0
16:00:00	1100	889	466	1355	29.23	44.57	0.0491	3.7710	0.5120	17.0	83.0
17:00:00	2000	1310	690	2000	29.11	44.45	0.0779	5.6030	0.7500	11.0	89.0
18:00:00	2400	1563	837	2400	29.07	44.64	0.0954	6.6100	0.9070	9.0	91.0
19:00:00	2400	1563	837	2400	29.07	44.64	0.0954	6.6100	0.9070	9.0	91.0
20:00:00	2400	1563	837	2400	29.07	44.64	0.0954	6.6100	0.9070	9.0	91.0
21:00:00	2400	1563	837	2400	29.07	44.64	0.0954	6.6100	0.9070	9.0	91.0
22:00:00	2100	1373	727	2100	29.09	44.50	0.0828	5.8830	0.7900	10.0	90.0
23:00:00	2100	1373	727	2100	29.09	44.50	0.0828	5.8830	0.7900	10.0	90.0

Light orange cells highlight hours in which the gas-steam unit operates below its nominal load.

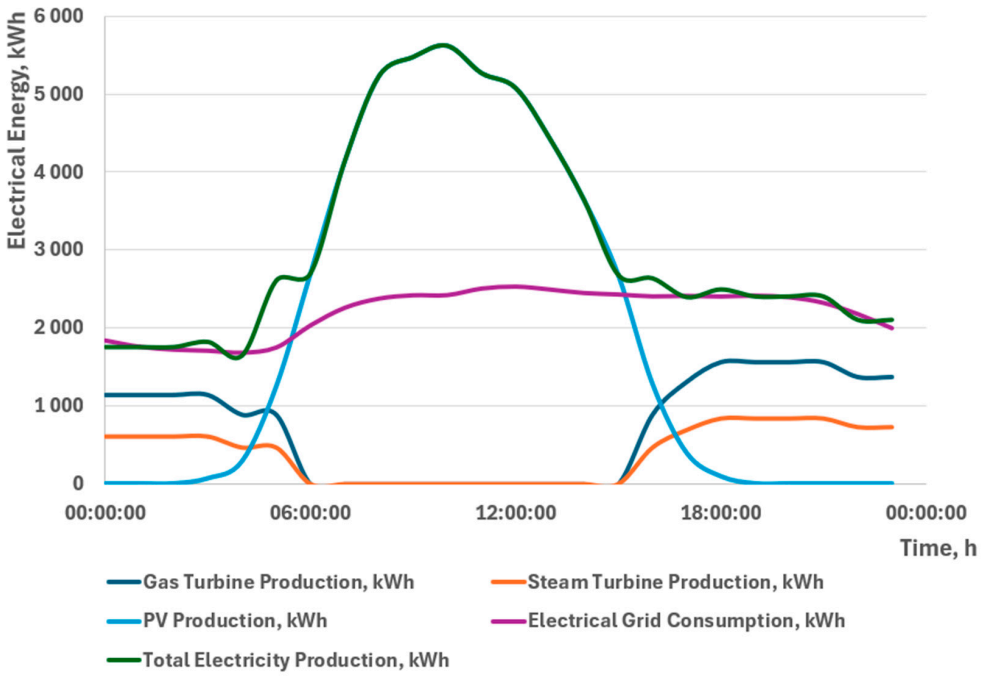

Appendix A.7. Average Hourly Energy Consumption-Production Balance in July

JULY											
Time	Consumption	GT Power Output	ST Power Output	Gas-Steam Power Output	GT Efficiency	Gas-Steam Efficiency	Fuel Mix Mass Flow	Exhaust Mass Flow	Live Steam Mass Flow	H_2 Mass Prop	CH_4 Mass Prop
	kWh	kWh	kWh	kWh	%	%	kg/s	kg/s	kg/s	%	%
00:00:00	1720	1124	596	1720	29.11	44.55	0.0669	4.8090	0.6500	11.0	89.0
01:00:00	1720	1124	596	1720	29.11	44.55	0.0669	4.8090	0.6500	11.0	89.0
02:00:00	1720	1124	596	1720	29.11	44.55	0.0669	4.8090	0.6500	11.0	89.0
03:00:00	1720	1124	596	1720	29.11	44.55	0.0669	4.8090	0.6500	11.0	89.0
04:00:00	1400	891	467	1358	29.15	44.41	0.0517	3.8020	0.5120	13.0	87.0
05:00:00	500	891	467	1358	29.15	44.41	0.0517	3.8020	0.5120	13.0	87.0
06:00:00	0	0	0	0	0.00	0.00	0.0000	0.0000	0.0000	0.0	0.0
07:00:00	0	0	0	0	0.00	0.00	0.0000	0.0000	0.0000	0.0	0.0
08:00:00	0	0	0	0	0.00	0.00	0.0000	0.0000	0.0000	0.0	0.0
09:00:00	0	0	0	0	0.00	0.00	0.0000	0.0000	0.0000	0.0	0.0
10:00:00	0	0	0	0	0.00	0.00	0.0000	0.0000	0.0000	0.0	0.0
11:00:00	0	0	0	0	0.00	0.00	0.0000	0.0000	0.0000	0.0	0.0
12:00:00	0	0	0	0	0.00	0.00	0.0000	0.0000	0.0000	0.0	0.0
13:00:00	0	0	0	0	0.00	0.00	0.0000	0.0000	0.0000	0.0	0.0
14:00:00	0	0	0	0	0.00	0.00	0.0000	0.0000	0.0000	0.0	0.0
15:00:00	0	0	0	0	0.00	0.00	0.0000	0.0000	0.0000	0.0	0.0
16:00:00	1100	891	467	1358	29.15	44.41	0.0517	3.8020	0.5120	13.0	87.0
17:00:00	2000	1305	695	2000	29.09	44.60	0.0786	5.5890	0.7560	10.0	90.0
18:00:00	2300	1504	796	2300	29.07	44.46	0.0918	6.4520	0.8630	9.0	91.0
19:00:00	2300	1504	796	2300	29.07	44.46	0.0918	6.4520	0.8630	9.0	91.0
20:00:00	2300	1504	796	2300	29.07	44.46	0.0918	6.4520	0.8630	9.0	91.0
21:00:00	2300	1504	796	2300	29.07	44.46	0.0918	6.4520	0.8630	9.0	91.0
22:00:00	2050	1346	704	2050	29.07	44.30	0.0822	5.7720	0.7660	9.0	91.0
23:00:00	2050	1346	704	2050	29.07	44.30	0.0822	5.7720	0.7660	9.0	91.0

Light orange cells highlight hours in which the gas-steam unit operates below its nominal load.

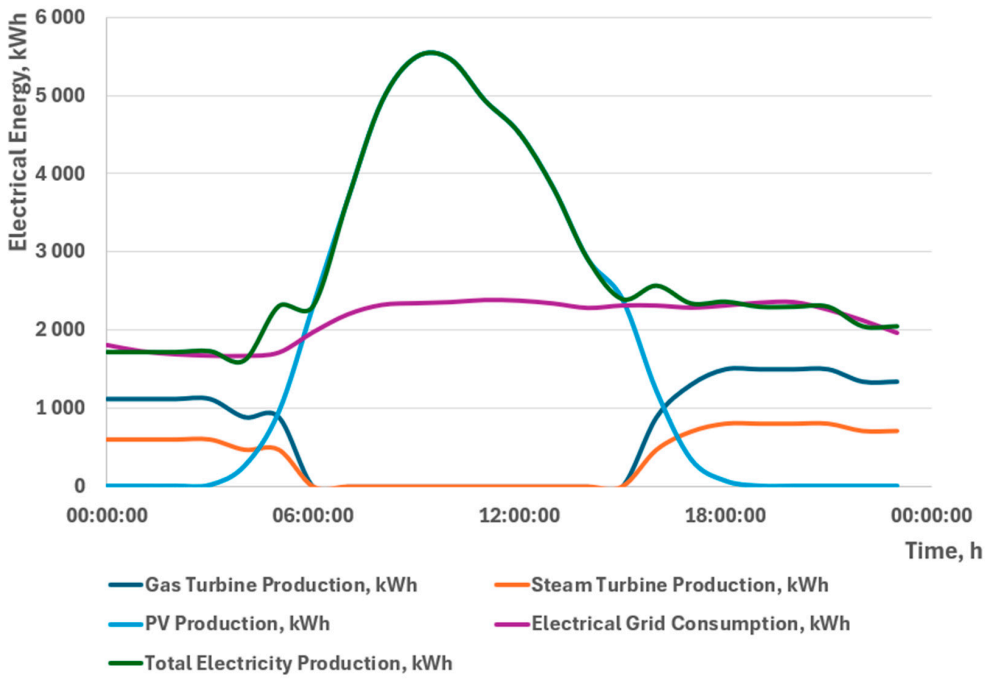

Appendix A.8. Average Hourly Energy Consumption-Production Balance in August

AUGUST											
Time	Consumption	GT Power Output	ST Power Output	Gas-Steam Power Output	GT Efficiency	Gas-Steam Efficiency	Fuel Mix Mass Flow	Exhaust Mass Flow	Live Steam Mass Flow	H_2 Mass Prop	Ch_4 Mass Prop
	kWh	kWh	kWh	kWh	%	%	kg/s	kg/s	kg/s	%	%
00:00:00	1550	1013	537	1550	29.05	44.44	0.0627	4.3530	0.5870	8.0	92.0
01:00:00	1550	1013	537	1550	29.05	44.44	0.0627	4.3530	0.5870	8.0	92.0
02:00:00	1550	1013	537	1550	29.05	44.44	0.0627	4.3530	0.5870	8.0	92.0
03:00:00	1550	1013	537	1550	29.05	44.44	0.0627	4.3530	0.5870	8.0	92.0
04:00:00	1550	1013	537	1550	29.05	44.44	0.0627	4.3530	0.5870	8.0	92.0
05:00:00	1000	887	466	1353	29.07	44.36	0.0542	3.8040	0.5120	9.0	91.0
06:00:00	0	0	0	0	0.00	0.00	0.0000	0.0000	0.0000	0.0	0.0
07:00:00	0	0	0	0	0.00	0.00	0.0000	0.0000	0.0000	0.0	0.0
08:00:00	0	0	0	0	0.00	0.00	0.0000	0.0000	0.0000	0.0	0.0
09:00:00	0	0	0	0	0.00	0.00	0.0000	0.0000	0.0000	0.0	0.0
10:00:00	0	0	0	0	0.00	0.00	0.0000	0.0000	0.0000	0.0	0.0
11:00:00	0	0	0	0	0.00	0.00	0.0000	0.0000	0.0000	0.0	0.0
12:00:00	0	0	0	0	0.00	0.00	0.0000	0.0000	0.0000	0.0	0.0
13:00:00	0	0	0	0	0.00	0.00	0.0000	0.0000	0.0000	0.0	0.0
14:00:00	0	0	0	0	0.00	0.00	0.0000	0.0000	0.0000	0.0	0.0
15:00:00	500	887	466	1353	29.07	44.36	0.0542	3.8040	0.5120	9.0	91.0
16:00:00	1650	1083	567	1650	29.03	44.25	0.0679	4.6580	0.6200	7.0	93.0
17:00:00	2200	1435	765	2200	28.98	44.45	0.0925	6.1920	0.8310	5.0	95.0
18:00:00	2400	1560	840	2400	28.98	44.58	0.1006	6.7370	0.9100	5.0	95.0
19:00:00	2400	1560	840	2400	28.98	44.58	0.1006	6.7370	0.9100	5.0	95.0
20:00:00	2400	1560	840	2400	28.98	44.58	0.1006	6.7370	0.9100	5.0	95.0
21:00:00	2400	1560	840	2400	28.98	44.58	0.1006	6.7370	0.9100	5.0	95.0
22:00:00	2000	1304	696	2000	28.99	44.48	0.0835	5.6230	0.7570	5.5	94.5
23:00:00	2000	1304	696	2000	28.99	44.48	0.0835	5.6230	0.7570	5.5	94.5

Light orange cells highlight hours in which the gas-steam unit operates below its nominal load.

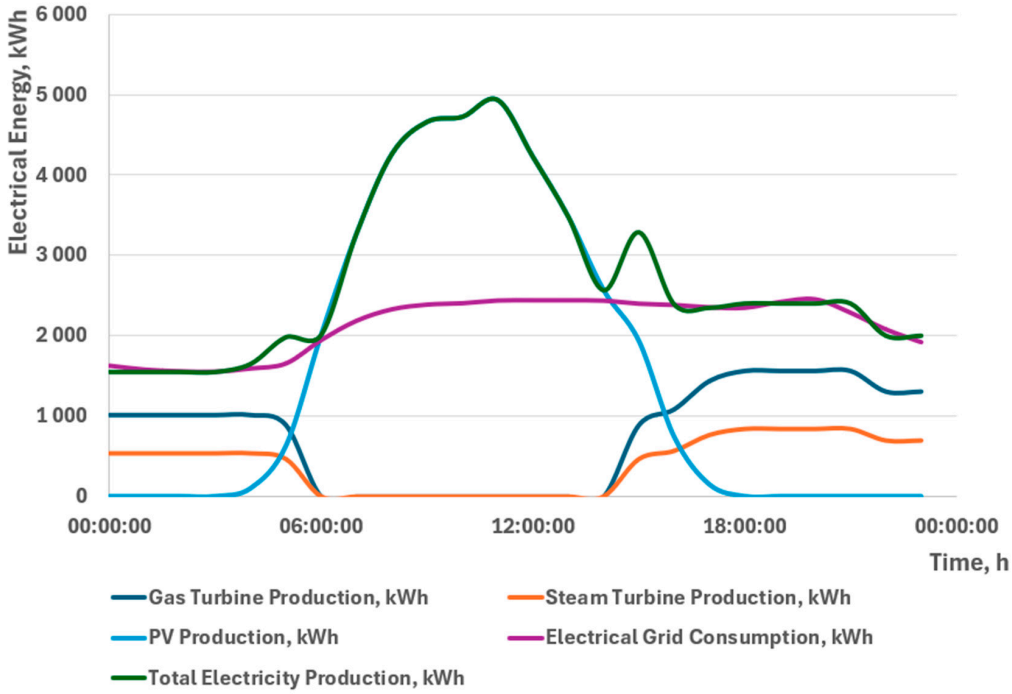

Appendix A.9. Average Hourly Energy Consumption-Production Balance in September

SEPTEMBER											
Time	Consumption	GT Power Output	ST Power Output	Gas-Steam Power Output	GT Efficiency	Gas-Steam Efficiency	Fuel Mix Mass Flow	Exhaust Mass Flow	Live Steam Mass Flow	H_2 Mass Prop	CH_4 Mass Prop
	kWh	kWh	kWh	kWh	%	%	kg/s	kg/s	kg/s	%	%
00:00:00	1700	1114	586	1700	29.11	44.44	0.0663	4.7660	0.6400	11.0	89.0
01:00:00	1700	1114	586	1700	29.11	44.44	0.0663	4.7660	0.6400	11.0	89.0
02:00:00	1700	1114	586	1700	29.11	44.44	0.0663	4.7660	0.6400	11.0	89.0
03:00:00	1700	1114	586	1700	29.11	44.44	0.0663	4.7660	0.6400	11.0	89.0
04:00:00	1700	1114	586	1700	29.11	44.44	0.0663	4.7660	0.6400	11.0	89.0
05:00:00	1400	891	467	1358	29.15	44.41	0.0517	3.8020	0.5120	13.0	87.0
06:00:00	0	0	0	0	0.00	0.00	0.0000	0.0000	0.0000	0.0	0.0
07:00:00	0	0	0	0	0.00	0.00	0.0000	0.0000	0.0000	0.0	0.0
08:00:00	0	0	0	0	0.00	0.00	0.0000	0.0000	0.0000	0.0	0.0
09:00:00	0	0	0	0	0.00	0.00	0.0000	0.0000	0.0000	0.0	0.0
10:00:00	0	0	0	0	0.00	0.00	0.0000	0.0000	0.0000	0.0	0.0
11:00:00	0	0	0	0	0.00	0.00	0.0000	0.0000	0.0000	0.0	0.0
12:00:00	0	0	0	0	0.00	0.00	0.0000	0.0000	0.0000	0.0	0.0
13:00:00	0	0	0	0	0.00	0.00	0.0000	0.0000	0.0000	0.0	0.0
14:00:00	0	0	0	0	0.00	0.00	0.0000	0.0000	0.0000	0.0	0.0
15:00:00	850	891	467	1358	29.15	44.41	0.0517	3.8020	0.5120	13.0	87.0
16:00:00	2200	1441	759	2200	29.03	44.36	0.8914	6.1890	0.8240	8.0	92.0
17:00:00	2450	1604	846	2450	29.03	44.35	0.1006	6.9010	0.9170	7.0	93.0
18:00:00	2450	1604	846	2450	29.03	44.35	0.1006	6.9010	0.9170	7.0	93.0
19:00:00	2450	1604	846	2450	29.03	44.35	0.1006	6.9010	0.9170	7.0	93.0
20:00:00	2450	1604	846	2450	29.03	44.35	0.1006	6.9010	0.9170	7.0	93.0
21:00:00	2250	1467	783	2250	29.03	44.57	0.0908	6.3010	0.8500	8.0	92.0
22:00:00	2000	1305	695	2000	29.07	44.54	0.0797	5.6000	0.7550	9.0	91.0
23:00:00	2000	1305	695	2000	29.07	44.54	0.0797	5.6000	0.7550	9.0	91.0

Light orange cells highlight hours in which the gas-steam unit operates below its nominal load.

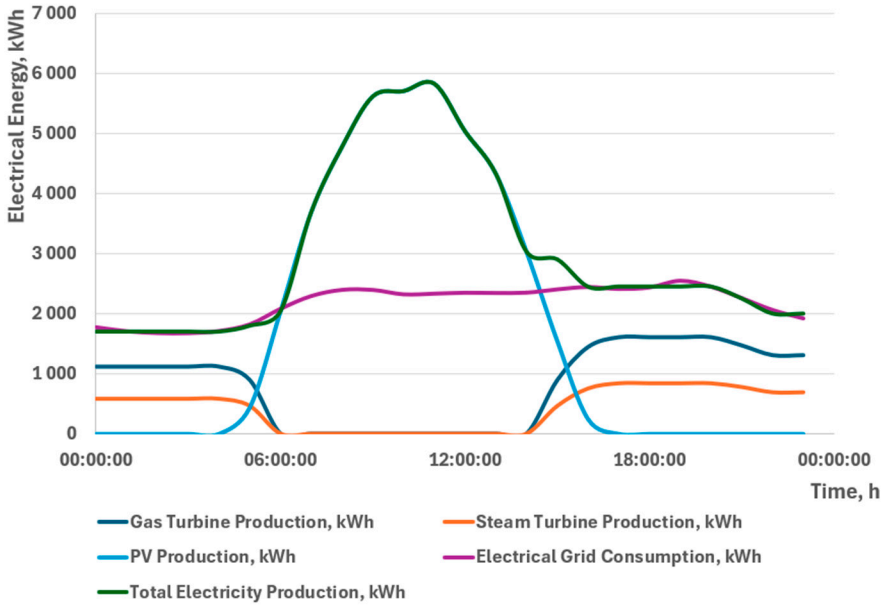

Appendix A.10. Average Hourly Energy Consumption-Production Balance in October

OCTOBER									
Time	**Consumption**	**GT Power Output**	**ST Power Output**	**Gas-Steam Power Output**	**GT Efficiency**	**Gas-Steam Efficiency**	**Biomethan Mass Flow**	**Exhaust Mass Flow**	**Live Steam Mass Flow**
	kWh	**kWh**	**kWh**	**kWh**	**%**	**%**	**kg/s**	**kg/s**	**kg/s**
00:00:00	1900	1235	665	1900	28.85	44.39	0.0855	5.3760	0.7240
01:00:00	1900	1235	665	1900	28.85	44.39	0.0855	5.3760	0.7240
02:00:00	1900	1235	665	1900	28.85	44.39	0.0855	5.3760	0.7240
03:00:00	1900	1235	665	1900	28.85	44.39	0.0855	5.3760	0.7240
04:00:00	1900	1235	665	1900	28.85	44.39	0.0855	5.3760	0.7240
05:00:00	1900	1235	665	1900	28.85	44.39	0.0855	5.3760	0.7240
06:00:00	1700	1106	594	1700	28.85	44.32	0.0766	4.8170	0.6470
07:00:00	1000	875	467	1342	28.85	44.23	0.0606	3.8110	0.5120
08:00:00	400	875	467	1342	28.85	44.23	0.0606	3.8110	0.5120
09:00:00	400	875	467	1342	28.85	44.23	0.0606	3.8110	0.5120
10:00:00	0	0	0	0	0.00	0.00	0.0000	0.0000	0.0000
11:00:00	0	0	0	0	0.00	0.00	0.0000	0.0000	0.0000
12:00:00	600	875	467	1342	28.85	44.23	0.0606	3.8110	0.5120
13:00:00	900	875	467	1342	28.85	44.23	0.0606	3.8110	0.5120
14:00:00	1500	980	520	1500	28.85	44.17	0.0679	4.2680	0.5700
15:00:00	2200	1429	771	2200	28.85	44.43	0.0990	6.2190	0.8370
16:00:00	2550	1654	896	2550	28.85	44.48	0.1146	7.2000	0.9700
17:00:00	2550	1654	896	2550	28.85	44.48	0.1146	7.2000	0.9700
18:00:00	2550	1654	896	2550	28.85	44.48	0.1146	7.2000	0.9700
19:00:00	2550	1654	896	2550	28.85	44.48	0.1146	7.2000	0.9700
20:00:00	2550	1654	896	2550	28.85	44.48	0.1146	7.2000	0.9700
21:00:00	2550	1654	896	2550	28.85	44.48	0.1146	7.2000	0.9700
22:00:00	2100	1365	735	2100	28.85	44.41	0.0946	5.9450	0.8000
23:00:00	2100	1365	735	2100	28.85	44.41	0.0946	5.9450	0.8000

Light orange cells highlight hours in which the gas-steam unit operates below its nominal load.

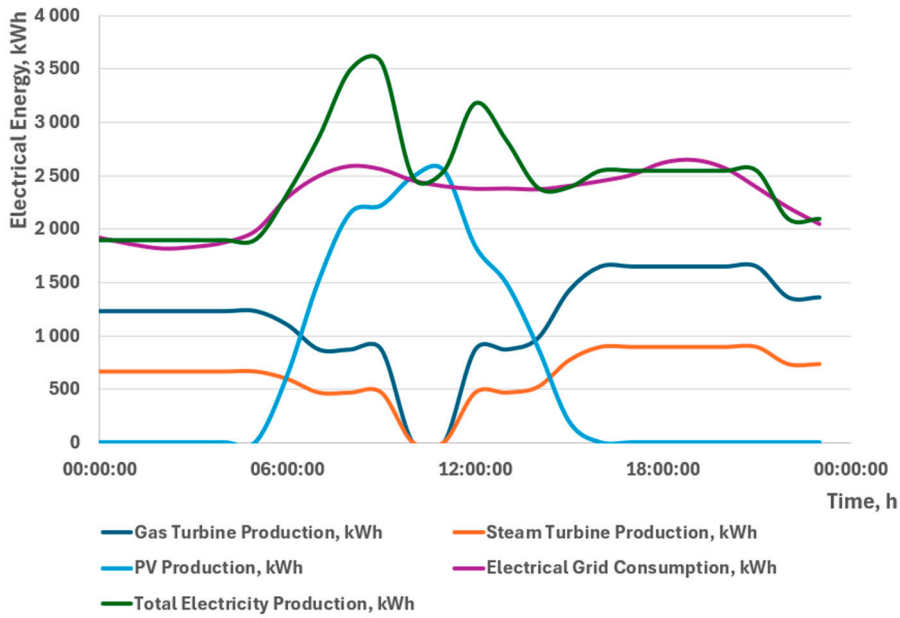

Appendix A.11. Average Hourly Energy Consumption-Production Balance in November

NOVEMBER									
Time	**Consumption**	**GT Power Output**	**ST Power Output**	**Gas-Steam Power Output**	**GT Efficiency**	**Gas-Steam Efficiency**	**Biomethan Mass Flow**	**Exhaust Mass Flow**	**Live Steam Mass Flow**
	kWh	**kWh**	**kWh**	**kWh**	**%**	**%**	**kg/s**	**kg/s**	**kg/s**
00:00:00	1900	1235	665	1900	28.85	44.39	0.0855	5.3760	0.7240
01:00:00	1900	1235	665	1900	28.85	44.39	0.0855	5.3760	0.7240
02:00:00	1900	1235	665	1900	28.85	44.39	0.0855	5.3760	0.7240
03:00:00	1900	1235	665	1900	28.85	44.39	0.0855	5.3760	0.7240
04:00:00	1900	1235	665	1900	28.85	44.39	0.0855	5.3760	0.7240
05:00:00	1900	1235	665	1900	28.85	44.39	0.0855	5.3760	0.7240
06:00:00	2200	1429	771	2200	28.85	44.43	0.0990	6.2190	0.8370
07:00:00	1900	1235	665	1900	28.85	44.39	0.0855	5.3760	0.7240
08:00:00	1400	913	487	1400	28.85	44.25	0.0632	3.9730	0.5340
09:00:00	1400	913	487	1400	28.85	44.25	0.0632	3.9730	0.5340
10:00:00	850	875	467	1342	28.85	44.23	0.0606	3.8110	0.5120
11:00:00	1150	875	467	1342	28.85	44.23	0.0606	3.8110	0.5120
12:00:00	1500	980	520	1500	28.85	44.17	0.0679	4.2680	0.5700
13:00:00	2100	1365	735	2100	28.85	44.41	0.0946	5.9450	0.8000
14:00:00	2650	1722	928	2650	28.85	44.38	0.1193	7.4990	1.0030
15:00:00	2650	1722	928	2650	28.85	44.38	0.1193	7.4990	1.0030
16:00:00	2650	1722	928	2650	28.85	44.38	0.1193	7.4990	1.0030
17:00:00	2650	1722	928	2650	28.85	44.38	0.1193	7.4990	1.0030
18:00:00	2650	1722	928	2650	28.85	44.38	0.1193	7.4990	1.0030
19:00:00	2650	1722	928	2650	28.85	44.38	0.1193	7.4990	1.0030
20:00:00	2650	1722	928	2650	28.85	44.38	0.1193	7.4990	1.0030
21:00:00	2650	1722	928	2650	28.85	44.38	0.1193	7.4990	1.0030
22:00:00	2200	1429	771	2200	28.85	44.43	0.0990	6.2190	0.8370
23:00:00	2200	1429	771	2200	28.85	44.43	0.0990	6.2190	0.8370

Light orange cells highlight hours in which the gas-steam unit operates below its nominal load.

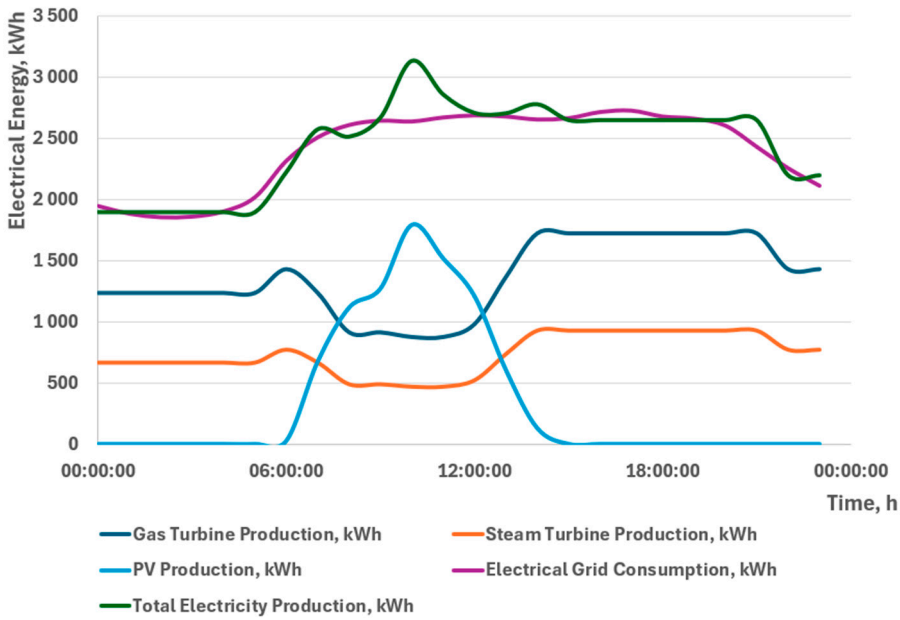

Appendix A.12. Average Hourly Energy Consumption-Production Balance in December

DECEMBER									
Time	Consumption	GT Power Output	ST Power Output	Gas-Steam Power Output	GT Efficiency	Gas-Steam Efficiency	Biomethan Mass Flow	Exhaust Mass Flow	Live Steam Mass Flow
	kWh	kWh	kWh	kWh	%	%	kg/s	kg/s	kg/s
00:00:00	2000	1301	699	2000	28.85	44.38	0.0901	5.6600	0.7610
01:00:00	2000	1301	699	2000	28.85	44.38	0.0901	5.6600	0.7610
02:00:00	2000	1301	699	2000	28.85	44.38	0.0901	5.6600	0.7610
03:00:00	2000	1301	699	2000	28.85	44.38	0.0901	5.6600	0.7610
04:00:00	2000	1301	699	2000	28.85	44.38	0.0901	5.6600	0.7610
05:00:00	2000	1301	699	2000	28.85	44.38	0.0901	5.6600	0.7610
06:00:00	2500	1623	877	2500	28.85	44.46	0.1124	7.0620	0.9500
07:00:00	2500	1623	877	2500	28.85	44.46	0.1124	7.0620	0.9500
08:00:00	1850	1202	648	1850	28.85	44.40	0.0833	5.2330	0.7050
09:00:00	1850	1202	648	1850	28.85	44.40	0.0833	5.2330	0.7050
10:00:00	2150	1398	752	2150	28.85	44.37	0.0969	6.0870	0.8160
11:00:00	2150	1398	752	2150	28.85	44.37	0.0969	6.0870	0.8160
12:00:00	2150	1398	752	2150	28.85	44.37	0.0969	6.0870	0.8160
13:00:00	2600	1685	915	2600	28.85	44.52	0.1167	7.3370	0.9900
14:00:00	2800	1817	983	2800	28.85	44.46	0.1259	7.9110	1.0630
15:00:00	2800	1817	983	2800	28.85	44.46	0.1259	7.9110	1.0630
16:00:00	2800	1817	983	2800	28.85	44.46	0.1259	7.9110	1.0630
17:00:00	2800	1817	983	2 800	28.85	44.46	0.1259	7.9110	1.0630
18:00:00	2800	1817	983	2 800	28.85	44.46	0.1259	7.9110	1.0630
19:00:00	2800	1817	983	2 800	28.85	44.46	0.1259	7.9110	1.0630
20:00:00	2800	1817	983	2 800	28.85	44.46	0.1259	7.9110	1.0630
21:00:00	2550	1654	896	2 550	28.85	44.48	0.1146	7.2000	0.9700
22:00:00	2300	1493	807	2 300	28.85	44.44	0.1035	6.5030	0.8750
23:00:00	2300	1493	807	2 300	28.85	44.44	0.1035	6.5030	0.8750

References

1. Bakkaloglu, S.; Hawkes, A. A comparative study of biogas and biomethane with natural gas and hydrogen alternatives. *Energy Environ. Sci.* **2024**, *17*, 1482–1496. [CrossRef]
2. D'Adamo, I.; Ribichini, M.; Tsagarakis, K.P. Biomethane as an energy resource for achieving sustainable production: Economic assessments and policy implications. *Sustain. Prod. Consum.* **2023**, *35*, 13–27. [CrossRef]
3. Pilarski, K.; Pilarska, A.A.; Pietrzak, M.B. Biogas Production in Agriculture: Technological, Environmental, and Socio-Economic Aspects. *Energies* **2025**, *18*, 5844. [CrossRef]
4. Swinbourn, R.; Li, C.; Wang, F. A Comprehensive Review on Biomethane Production from Biogas Separation and its Techno-Economic Assessments. *ChemSusChem* **2024**, *17*, e202400779. [CrossRef] [PubMed]
5. IEA An Introduction to Biogas and Biomethane, The Outlook for Biogas and Biomethane to 2040 n.d. Available online: https://www.iea.org/reports/outlook-for-biogas-and-biomethane-prospects-for-organic-growth/an-introduction-to-biogas-and-biomethane (accessed on 12 May 2025).
6. Mignogna, D.; Ceci, P.; Cafaro, C.; Corazzi, G.; Avino, P. Production of Biogas and Biomethane as Renewable Energy Sources: A Review. *Appl. Sci.* **2023**, *13*, 10219. [CrossRef]
7. Adnane, I.; Taoumi, H.; Lahrech, K.; Fertahi, S.E.-D.; Ghodbane, M. From waste to resource: Biogas and digestate valorization strategies for sustainable energy and agriculture. *Biomass Bioenergy* **2025**, *200*, 108006. [CrossRef]
8. Piechota, G.; Igliński, B. Biomethane in Poland—Current Status, Potential, Perspective and Development. *Energies* **2021**, *14*, 1517. [CrossRef]
9. Sulewski, P.; Ignaciuk, W.; Szymańska, M.; Wąs, A. Development of the Biomethane Market in Europe. *Energies* **2023**, *16*, 2001. [CrossRef]
10. Chen, X.; Fu, W.; Hu, K.; Yin, G.; Liu, S.; Zhu, N.; Zhao, Y.; Cui, Z.; Yuan, X. Economic and environmental analysis: Straw biogas project operating at full load with dry yellow corn straw. *Bioresour. Technol.* **2025**, *426*, 132335. [CrossRef]
11. Li, P.; He, C.; Li, G.; Ding, P.; Lan, M.; Gao, Z.; Jiao, Y. Biological pretreatment of corn straw for enhancing degradation efficiency and biogas production. *Bioengineered* **2020**, *11*, 251–260. [CrossRef]
12. Guan, S.; He, C.; Li, P.; Li, P.; Hou, T.; Gao, Z.; Li, G.; Jiao, Y. Enhancement of Anaerobic Digestion of Corn Straw: Effect of Biological Pretreatment and Heating with Bio-Heat Recovery from Pretreatment. *Fermentation* **2024**, *10*, 160. [CrossRef]
13. Saboohi, Z.; Hosseini, S.E. Advancements in biogas production: Process optimization and innovative plant operations. *Clean Energy* **2025**, *9*, 52–65. [CrossRef]
14. Rodrigues, B.C.G.; de Mello, B.S.; Grangeiro, L.C.; Dussan, K.J.; Sarti, A. The most important technologies and highlights for biogas production worldwide. *J. Air Waste Manag. Assoc.* **2024**, *75*, 87–108. [CrossRef] [PubMed]
15. Kapłan, M.; Klimek, K.; Syrotyuk, S.; Konieczny, R.; Jura, B.; Smoliński, A.; Szymenderski, J.; Budnik, K.; Anders, D.; Dybek, B.; et al. Raw biogas desulphurization using the adsorption-absorption technique for a pilot production of agricultural biogas from pig slurry in Poland. *Energies* **2021**, *14*, 5929. [CrossRef]
16. Siddiki, S.Y.A.; Uddin, M.; Mofijur, M.; Fattah, I.; Ong, H.C.; Lam, S.S.; Kumar, P.S.; Ahmed, S. Theoretical calculation of biogas production and greenhouse gas emission reduction potential of livestock, poultry and slaughterhouse waste in Bangladesh. *J. Environ. Chem. Eng.* **2021**, *9*, 105204. [CrossRef]
17. Rauch, J.; Haloua, F. Calorific value of biomethane: Comparative measurements using reference gas calorimeters. *J. Phys. Conf. Ser.* **2018**, *1065*, 202007. [CrossRef]
18. Adnan, A.I.; Ong, M.Y.; Nomanbhay, S.; Chew, K.W.; Show, P.L. Technologies for biogas upgrading to biomethane: A review. *Bioengineering* **2019**, *6*, 92. [CrossRef]
19. Elsayed, A.; Kakar, F.L.; Marcus, A.; AlSayed, A.; Zagloul, M.S.; Muller, C.; Bell, K.Y.; Santoro, D.; Norton, J.; Elbeshbishy, E. Application of additives for anaerobic digestion intensification: A comprehensive review on improving biogas production and methane yield. *Appl. Energy* **2025**, *381*, 125202. [CrossRef]
20. Moltames, R.; Noorollahi, Y.; Yousefi, H.; Azizimehr, B.; Naseri, A. Assessment of potential sites for biogas production plants from domestic, agricultural, and livestock waste. *Fuel Commun.* **2025**, *22*, 100132. [CrossRef]
21. Green, M.A.; Dunlop, E.D.; Yoshita, M.; Kopidakis, N.; Bothe, K.; Siefer, G.; Hao, X. Solar cell efficiency tables (Version 63). *Prog. Photovolt. Res. Appl.* **2024**, *32*, 3–13. [CrossRef]
22. Santos, L.d.O.; AlSkaif, T.; Barroso, G.C.; de Carvalho, P.C.M. Photovoltaic power estimation and forecast models integrating physics and machine learning: A review on hybrid techniques. *Sol. Energy* **2024**, *284*, 113044. [CrossRef]
23. Luo, C.; Al-Messabi, N.; Kuang, Z.; Ma, C.; El-Amin, I.; Deng, H.; Li, Y. Photovoltaic system modeling and forecasting techniques: A survey. *Eng. Appl. Artif. Intell.* **2025**, *162*, 112516. [CrossRef]
24. Al Humairi, A.; El Asri, H.; Al Hemyari, Z.A.; Jung, P. A Robust Modeling Analysis of Environmental Factors Influencing the Direct Current, Power, and Voltage of Photovoltaic Systems. *Electronics* **2025**, *14*, 2647. [CrossRef]
25. Alfaris, A.; Akroot, A.; Alqaed, S.; Almehmadi, F.A. Performance analysis of integrated solar and natural gas combined cycle power plants in high solar potential regions. *Sci. Rep.* **2025**, *15*, 1–21. [CrossRef]

26. Reza, M.; Fattah, I.; Wang, J.; Hannan, M.; Zainal, B.; Ong, H.C.; Mahlia, T. Hydrogen-based hybrid energy system: A review of technologies, optimization approaches, objectives, constraints, applications, and outstanding issues. *Renew. Sustain. Energy Rev.* **2026**, *226*, 116192. [CrossRef]
27. Thai, C.; Brouwer, J. Decarbonizing a solar PV and gas turbine microgrid with hydrogen and batteries. *Energy Convers. Manag.* **2023**, *292*, 117391. [CrossRef]
28. Li, C.; Yang, T.; Cai, W.; Agbossou, K.; Bénard, P.; Chahine, R.; Zong, Y.; Li, Y.; Su, S.; Li, G.; et al. A comprehensive review of hydrogen integrated hybrid renewable energy systems: Configurations, models, simulation and optimization with artificial intelligence. *Green Energy Resour.* 2025; *in press*. [CrossRef]
29. Kanz, O.; Bittkau, K.; Ding, K.; Rau, U.; Reinders, A. Review and Harmonization of the Life-Cycle Global Warming Impact of PV-Powered Hydrogen Production by Electrolysis. *Front. Electron.* **2021**, *2*, 711103. [CrossRef]
30. Dawood, F.; Shafiullah, G.M.; Anda, M. Stand-alone microgrid with 100% renewable energy: A case study with hybrid solar pv-battery-hydrogen. *Sustainability* **2020**, *12*, 2047. [CrossRef]
31. Pavić, I.; Čović, N.; Pandžić, H. PV–battery-hydrogen plant: Cutting green hydrogen costs through multi-market positioning. *Appl. Energy* **2022**, *328*, 120103. [CrossRef]
32. Şevik, S. Techno-economic evaluation of a grid-connected PV-trigeneration-hydrogen production hybrid system on a university campus. *Int. J. Hydrogen Energy* **2022**, *47*, 23935–23956. [CrossRef]
33. Lv, X.; Li, X.; Xu, C. A robust optimization model for capacity configuration of PV/battery/hydrogen system considering multiple uncertainties. *Int. J. Hydrogen Energy* **2023**, *48*, 7533–7548. [CrossRef]
34. Lin, L.; Ou, K.; Lin, Q.; Xing, J.; Wang, Y.X. Two-stage multi-strategy decision-making framework for capacity configuration optimization of grid-connected PV/battery/hydrogen integrated energy system. *J. Energy Storage* **2024**, *97*, 112862. [CrossRef]
35. Zhou, L.; Song, A.; Zhou, Y. Electrification and hydrogenation on a PV-battery-hydrogen energy flexible community for carbon–neutral transformation with transient aging and collaboration operation. *Energy Convers. Manag.* **2024**, *300*, 117984. [CrossRef]
36. Li, J.; Liang, H.; Zheng, Z.; Teng, L.; Zhang, Z.; Gao, Z.; Luo, Y.; Zhang, C.; Jiang, L. A critical review of China's hydrogen supply chain and equipment. *Int. J. Hydrogen Energy* **2025**, *180*, 151737. [CrossRef]
37. Sebbahi, S.; Assila, A.; Belghiti, A.A.; Laasri, S.; Kaya, S.; Hlil, E.K.; Rachidi, S.; Hajjaji, A. A comprehensive review of recent advances in alkaline water electrolysis for hydrogen production. *Int. J. Hydrogen Energy* **2024**, *82*, 583–599. [CrossRef]
38. Zaccara, A.; Petrucciani, A.; Matino, I.; Branca, T.A.; Dettori, S.; Iannino, V.; Colla, V.; Bampaou, M.; Panopoulos, K. Renewable hydrogen production processes for the off-gas valorization in integrated steelworks through hydrogen intensified methane and methanol syntheses. *Metals* **2020**, *10*, 1535. [CrossRef]
39. El-Shafie, M. Hydrogen production by water electrolysis technologies: A review. *Results Eng.* **2023**, *20*, 101426. [CrossRef]
40. Pinto, R.; Oliveira, M.; Borges, A. An experimentally validated model of electrolyte effects in alkaline water electrolysis. *Sci. Rep.* **2025**, *15*, 41865. [CrossRef]
41. Sánchez, M.; Amores, E.; Abad, D.; Rodríguez, L.; Clemente-Jul, C. Aspen Plus model of an alkaline electrolysis system for hydrogen production. *Int. J. Hydrogen Energy* **2020**, *45*, 3916–3929. [CrossRef]
42. van der Does, W.L.; Valle, N.; Haverkort, J.W. Multiphase alkaline water electrolysis simulations: The need for a solid pressure model to explain experimental bubble overpotentials. *Int. J. Hydrogen Energy* **2025**, *102*, 295–303. [CrossRef]
43. Terlouw, T.; Bauer, C.; McKenna, R.; Mazzotti, M. Large-scale hydrogen production via water electrolysis: A techno-economic and environmental assessment. *Energy Environ. Sci.* **2022**, *15*, 3583–3602. [CrossRef]
44. Mekonnin, A.S.; Wacławiak, K.; Humayun, M.; Zhang, S.; Ullah, H. Hydrogen Storage Technology, and Its Challenges: A Review. *Catalysts* **2025**, *15*, 260. [CrossRef]
45. Su, Y.; Lv, H.; Zhou, W.; Zhang, C. Review of the hydrogen permeability of the liner material of type iv on-board hydrogen storage tank. *World Electr. Veh. J.* **2021**, *12*, 130. [CrossRef]
46. Nivedhitha, K.; Beena, T.; Banapurmath, N.; Umarfarooq, M.; Ramasamy, V.; Soudagar, M.E.M.; Ağbulut, Ü. Advances in hydrogen storage with metal hydrides: Mechanisms, materials, and challenges. *Int. J. Hydrogen Energy* **2024**, *61*, 1259–1273. [CrossRef]
47. Mulky, L.; Srivastava, S.; Lakshmi, T.; Sandadi, E.R.; Gour, S.; Thomas, N.A.; Priya, S.S.; Sudhakar, K. An overview of hydrogen storage technologies—Key challenges and opportunities. *Mater. Chem. Phys.* **2024**, *325*, 129710. [CrossRef]
48. Hydrogen Research Projects—Germany 2024. 2024. Available online: https://www.dvgw.de/medien/dvgw/en/publications/wasserstoff-forschungsprojekte-dvgw-2024-engl.pdf (accessed on 12 May 2025).
49. DESSERT Project—Advancing Sustainable Hydrogen Storage Technology. Available online: https://hydrogen-central.com/dessert-project-kicks-off-advancing-sustainable-hydrogen-storage-technology/?utm_source=chatgpt.com 2024 (accessed on 12 May 2025).

50. EU Clean Hydrogen Partnership. Available online: https://www.clean-hydrogen.europa.eu/media/news/31-new-projects-advancing-research-and-innovation-hydrogen-technologies-2024-03-11_en?utm_source=chatgpt.com n.d (accessed on 12 May 2025).
51. Tarkowski, R. Underground hydrogen storage: Characteristics and prospects. *Renew. Sustain. Energy Rev.* **2019**, *105*, 86–94. [CrossRef]
52. Zivar, D.; Kumar, S.; Foroozesh, J. Underground hydrogen storage: A comprehensive review. *Int. J. Hydrogen Energy* **2021**, *46*, 23436–23462. [CrossRef]
53. Alhuyi Nazari, M.; Fahim Alavi, M.; Salem, M.; Assad, M.E.H. Utilization of hydrogen in gas turbines: A comprehensive review. *Int. J. Low-Carbon Technol.* **2022**, *17*, 513–519. [CrossRef]
54. Zhou, H.; Xue, J.; Gao, H.; Ma, N. Hydrogen-fueled gas turbines in future energy system. *Int. J. Hydrogen Energy* **2024**, *64*, 569–582. [CrossRef]
55. Langston, L.S. Hydrogen Fueled Gas Turbines Available to Purchase. *Mech. Eng.* **2019**, *141*, 52–54. [CrossRef]
56. Abbass, A. Hydrogen Integration in Gas Turbines: OEM Innovations and Challenges in Advancing Sustainable Energy Systems. *J. Manag.* **2025**, *2*, 99–108. [CrossRef]
57. Abdelhafez, A.; Abdelhalim, A.; Abdulrahman, G.A.Q.; Haque, M.A.; Habib, M.A.; Nemitallah, M.A. Stability, near flashback combustion dynamics, and NOx emissions of H2/N2/air flames in a micromixer-based model gas turbine combustor. *Int. J. Hydrogen Energy* **2024**, *61*, 102–112. [CrossRef]
58. Sun, Y.; Zhang, Y.; Huang, M.; Li, Q.; Wang, W.; Zhao, D.; Cheng, S.; Deng, H.; Du, J.; Song, Y.; et al. Effect of hydrogen addition on the combustion and emission characteristics of methane under gas turbine relevant operating condition. *Fuel* **2022**, *324*, 124707. [CrossRef]
59. Cecere, D.; Giacomazzi, E.; Di Nardo, A.; Calchetti, G. Gas Turbine Combustion Technologies for Hydrogen Blends. *Energies* **2023**, *16*, 6829. [CrossRef]
60. Park, Y.; Choi, M.; Choi, G. Thermodynamic performance study of large-scale industrial gas turbine with methane/ammonia/hydrogen blended fuels. *Energy* **2023**, *282*, 128731. [CrossRef]
61. Singh, G.; Schreiner, B.D.J.; Sun, X.; Sethi, V. A review of hydrogen micromix combustion technologies for gas turbine applications. *Int. J. Hydrogen Energy* **2025**, *127*, 295–310. [CrossRef]
62. Atef, M.; Khatib, T.; Abdullah, M.F.; Romlie, M.F. Optimization of a Hybrid Solar PV and Gas Turbine Generator System Using the Loss of Load Probability Index. *Clean Technol.* **2020**, *2*, 240–251. [CrossRef]
63. Jia, K.; Liu, C.; Li, S.; Jiang, D. Modeling and optimization of a hybrid renewable energy system integrated with gas turbine and energy storage. *Energy Convers. Manag.* **2023**, *279*, 116763. [CrossRef]
64. De Robbio, R. Micro Gas Turbine Role in Distributed Generation with Renewable Energy Sources. *Energies* **2023**, *16*, 704. [CrossRef]
65. Li, J.; Liu, Z.; Ye, R. Current Status and Prospects of Gas Turbine Technology Application. *J. Phys. Conf. Ser.* **2021**, *2108*, 012009. [CrossRef]
66. Banihabib, R.; Assadi, M. A Hydrogen-Fueled Micro Gas Turbine Unit for Carbon-Free Heat and Power Generation. *Sustainability* **2022**, *14*, 13305. [CrossRef]
67. Banihabib, R.; Lingstädt, T.; Wersland, M.; Kutne, P.; Assadi, M. Development and testing of a 100 kW fuel-flexible micro gas turbine running on 100% hydrogen. *Int. J. Hydrogen Energy* **2024**, *49*, 92–111. [CrossRef]
68. Marin, G.E.; Titov, A.V.; Akhmetshin, A.R.; Ishalin, A.V. Increasing the efficiency of a conversion gas turbine engine by adding hydrogen to fuel gas. *Int. J. Hydrogen Energy* **2025**, *97*, 649–656. [CrossRef]
69. Marin, G.E.; Osipov, B.M.; Titov, A.V.; Akhmetshin, A.R. Simulation of the operation of a gas turbine installation of a thermal power plant with a hydrogen fuel production system. *Int. J. Hydrogen Energy* **2023**, *48*, 4543–4550. [CrossRef]
70. Marin, G.E.; Osipov, B.M.; Titov, A.V.; Akhmetshin, A.R. Gas turbine operating as part of a thermal power plant with hydrogen storages. *Int. J. Hydrogen Energy* **2023**, *48*, 33393–33400. [CrossRef]
71. Qi, X.; Kochan, O.; Ma, Z.; Siarry, P.; Królczyk, G.; Li, Z. Energy, exergy, exergoeconomic and exergoenvironmental analyses of a hybrid renewable energy system with hydrogen fuel cells. *Int. J. Hydrogen Energy* **2024**, *52*, 617–634. [CrossRef]
72. Öberg, S.; Odenberger, M.; Johnsson, F. Exploring the competitiveness of hydrogen-fueled gas turbines in future energy systems. *Int. J. Hydrogen Energy* **2022**, *47*, 624–644. [CrossRef]
73. Skabelund, B.B.; Jenkins, C.D.; Stechel, E.B.; Milcarek, R.J. Thermodynamic and emission analysis of a hydrogen/methane fueled gas turbine. *Energy Convers. Manag. X* **2023**, *19*, 100394. [CrossRef]
74. Głaszczka, A.; Jan Wardal, W.; Romaniuk, W. *Biogazownie Rolicze, Technologie Energii Odnawialnej*; MULTICO Oficyna Wydawnicza sp. z o.o.: Warsaw, Poland, 2020.

75. Harutyunyan, A.; Badyda, K.; Szablowski, Ł. Energy and exergy analysis of a hydrogen powered gas turbine operating in gas-steam system. *J. Phys. Conf. Ser.* **2024**, *2812*, 012009. [CrossRef]
76. Taher, M. *An Overview of ASME PTC 10-2022 on Performance Testing of Axial and Centrifugal Compressors*; American Society of Mechanical Engineers: New York, NY, USA, 2024.

Disclaimer/Publisher's Note: The statements, opinions and data contained in all publications are solely those of the individual author(s) and contributor(s) and not of MDPI and/or the editor(s). MDPI and/or the editor(s) disclaim responsibility for any injury to people or property resulting from any ideas, methods, instructions or products referred to in the content.